Effective normal stress alteration due to pore pressure changes induced by dynamic slip propagation on a plane between dissimilar materials

John W. Rudnicki[1] and James R. Rice[2]

Received 16 March 2006; accepted 11 July 2006; published 28 October 2006.

[1] Recent, detailed examinations of fault zones show that walls of faults are often bordered by materials that are different from each other and from the more uniform material farther away. In addition, they show that the ultracataclastic core of mature fault zones, where slip is concentrated, is less permeable to flow across it than the adjoining material of the damage zone. Inhomogeneous slip at the interface between materials with different poroelastic properties and permeabilities causes a change in pore pressure there. Because slip causes compression on one side of the fault wall and extension on the other, the pore pressure on the fault increases substantially when the compressed side is significantly more permeable and decreases when, instead, the extended side is more permeable. This change in pore pressure alters the effective normal stress on the slip plane in a way that is analogous to the normal stress alteration in sliding between elastically dissimilar solids. The magnitude of the effect due to induced pore pressure can be comparable to or larger than that induced by sliding between elastic solids with a dissimilarity of properties consistent with seismic observations. The induced pore pressure effect is increased by increasing contrast in permeability, but the normal stress alteration due to elastic contrast increases rapidly as the rupture velocity approaches the generalized Rayleigh velocity. Because the alteration in effective normal stress due to either effect can be positive or negative, depending on the contrast in properties, the two effects can augment or offset each other.

Citation: Rudnicki, J. W., and J. R. Rice (2006), Effective normal stress alteration due to pore pressure changes induced by dynamic slip propagation on a plane between dissimilar materials, *J. Geophys. Res.*, *111*, B10308, doi:10.1029/2006JB004396.

1. Introduction

[2] A number of recent field studies [*Chester et al.*, 1993; *Chester and Chester*, 1998; *Lockner et al.*, 2000; *Wibberley and Shimamoto*, 2003; *Sulem et al.*, 2004; *Noda and Shimamoto*, 2005] have identified the ultracataclastic cores of mature fault zones, where the slip is concentrated, and shown that the core is much less permeable to flow across it than is the adjoining material of the damage zone. Because slip causes compression on one side of the fault wall and extension on the other, the pore pressure tends to increase on the compressive side and decrease on the extensile. This strong gradient results in a pore pressure on the fault slip surface (treated as a plane) that depends on the difference in properties on the two sides. The pore pressure on the fault increases substantially when the compressed side is significantly more permeable, and decreases when, instead, the extended side is more permeable. An increase in pore pressure reduces the effective compressive stress and hence the frictional resistance to slip, whereas a decrease has the opposite effect. *Rudnicki and Koutsibelas* [1991] considered the case of identical properties on the two sides of a completely impermeable fault plane. Following a suggestion of J. R. Rice (personal communication, 1987), they argued that the pore pressure increase, rather than the decrease on the other side of the slip zone, affects the rupture propagation. Their interpretation emerges as the proper limit case here when there is a much more permeable material on the compressive side than on the extensile.

[3] This paper calculates the pore pressure induced by a dynamically propagating fault within the framework of the model used by *Rice et al.* [2005] (hereinafter referred to as RSP). The calculation is based on a model of discontinuous slip on a plane in an otherwise homogeneous poroelastic solid, but, in calculating the pore pressure change, we include the effects of differences in material properties in narrow damage and granulation zones along the fault walls. The pore pressure discontinuity predicted to occur across a completely impermeable slip plane idealizes the spatially rapid pore pressure variation that would occur across a narrow but finite width fault zone with, generally, different properties than the surrounding material (Figure 1). The

[1]Department of Mechanical Engineering and Department of Civil and Environmental Engineering, Northwestern University, Evanston, Illinois, USA.
[2]Department of Earth and Planetary Sciences and Division of Engineering and Applied Sciences, Harvard University, Cambridge, Massachusetts, USA.

0148-0227/06/2006JB004396$09.00

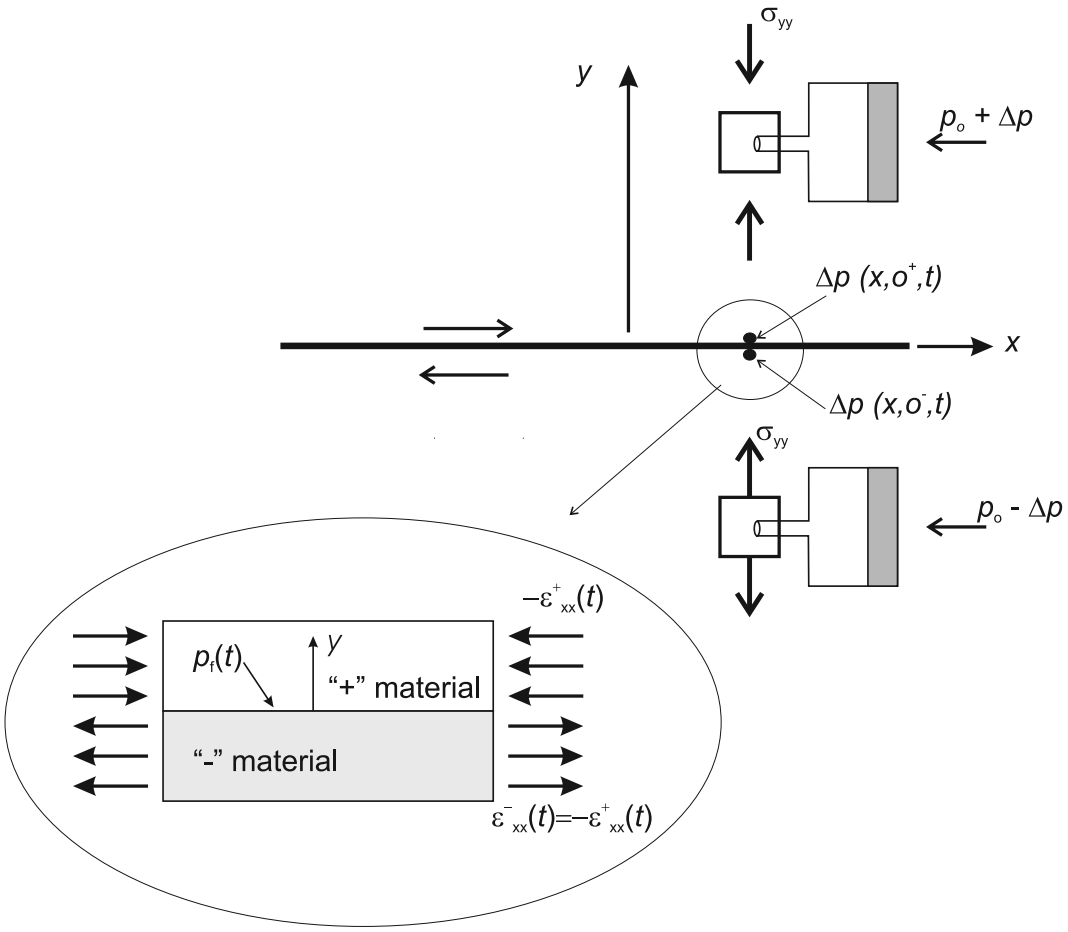

Figure 1. Schematic diagram showing that the pore pressure change is equal in magnitude and opposite in sign on the two sides of the slip plane. Inset shows a more elaborate near-fault model in which the fault plane is the boundary between two materials that may be different from the material farther from the fault. The layers shown in the inset are so narrow that they are idealized as experiencing a uniform fault-parallel strain ε_{xx} with the same magnitude but opposite signs on the two sides of the boundary (where slip occurs).

model treated in the main part of the paper considers the material on the two sides of the fault as homogeneous and simply assumes, as in the work by *Rudnicki and Koutsibelas* [1991], that the pore pressure on the compressive side controls strength. We show, however, in Appendix B that a more elaborate model of the near fault region can be included simply by modifying the coefficient of the pore pressure (Skempton's coefficient) in the main text.

[4] In the more elaborate model (Figure 1, inset), the permeability and poroelastic properties of the material on the two sides of the fault differ from each other and from the homogeneous material farther from the fault. This model is consistent with fault zone studies that show that the fault core is embedded in a damaged region that may extend several meters beyond the core [*Chester et al.*, 1993; *Chester and Chester*, 1998; *Wibberley and Shimamoto*, 2003] and that the slip surface is often coincident with the boundary between ultracataclasites of different origin (from host rocks on the two sides) or at a boundary between one of the ultracataclasites and damaged host rock [*Chester and Chester*, 1998]. These near-fault regions are, however, idealized as sufficiently narrow that they are subjected to fault parallel strains that are uniform but equal in magnitude and opposite in sign on the two sides of the material boundary. These are the same strains as would be present if the homogeneous material outside extended all the way to the slip plane. When the material on the compressive side of the fault is much more permeable than that on the extensile side, the model reduces to the impermeable slip plane idealization with pore pressure on the compressive side controlling strength.

[5] A result of the analysis is that the alteration of pore pressure and hence of effective normal stress on the fault is proportional to the along fault gradient of the slip. This is the same form as the alteration of normal stress due to heterogeneous slip between dissimilar elastic solids, an effect that has been widely studied in seismology [*Weertman*, 1980; *Andrews and Ben-Zion*, 1997; *Harris and Day*, 1997; *Cochard and Rice*, 2000; *Ben-Zion*, 2001; *Xia et al.*, 2005]. Consequently, we are able to compare the magnitude of the two effects. Their combination provides a more general framework for the inclusion of material heterogeneities, not only dissimilarity of the crustal blocks on the two sides of the fault but also the dissimilarity of permeability and poroelastic properties on the two sides of the slip surface. Because both effects may be of either sign, decreasing or

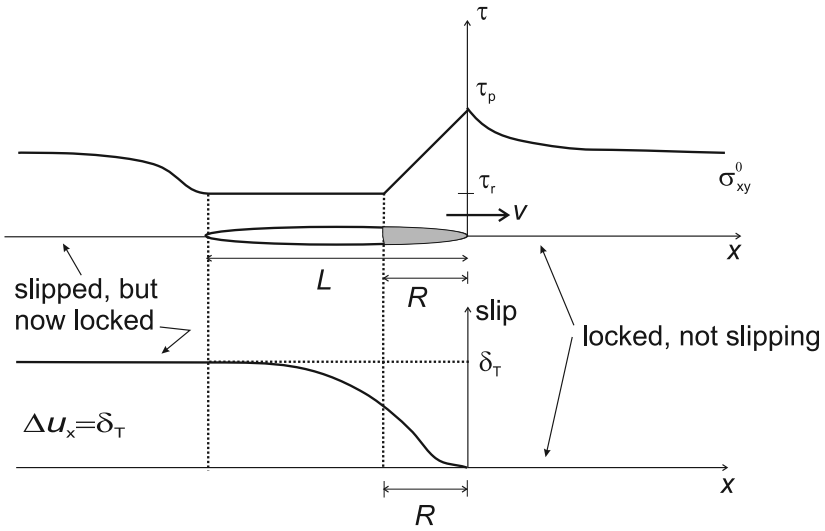

Figure 2. Schematic illustration of the cohesive zone, slip pulse model used by RSP.

increasing the effective normal stress on the fault, depending on the direction of slip and mismatch of properties, they can augment or offset each other.

2. Formulation

[6] RSP considered a propagating slip pulse of length L with slip weakening as shown in Figure 2. The pulse is propagating at a constant velocity v. The stress on the slip plane far ahead of the slipping zone is σ^0_{xy}. The frictional resistance to slip on the fault plane is given by

$$\tau = \tau^0(x) = \begin{cases} \tau_p + (\tau_p - \tau_r)(x/R), & -R \le x < 0 \\ \tau_r, & -L \le x < -R \end{cases} \quad (1)$$

The resistance weakens from a peak strength τ_p at initiation of slip to a residual strength τ_r at which large slip can occur. In a common interpretation (we mention a different one below), these strengths are assumed to be entirely frictional in origin such that τ can be expressed as

$$\tau = -f\bar{\sigma}_{yy}(x,0) = -f\left(\sigma_{yy}(x,0) + p(x,0)\right) \quad (2)$$

where f is a friction coefficient, $\sigma_{yy}(x, 0)$ is the total normal stress on the slip plane and $\bar{\sigma}_{yy}(x, 0)$ is the effective normal stress (both positive in tension), and $p(x, 0)$ is pore pressure. In the case considered in RSP, both $p(x, 0)$ and $\sigma_{yy}(x, 0)$ were constant, and hence also $\bar{\sigma}_{yy}(x, 0)$; in the generalization of this paper, only $\sigma_{yy}(x, 0)$ is constant, and that only when we consider materials of identical elastic properties on the two sides of the fault. Immediately in front of the slipping zone (at the onset of slip), the resistive stress is $\tau = \tau_p$, where $\tau_p = -f_s\bar{\sigma}_{yy}(x, 0)$ and f_s is a static coefficient of friction. The frictional resistance decreases with increasing slip and at a distance R behind the edge of the slipping zone reaches a residual value given by $\tau_r = -f_d\bar{\sigma}_{yy}(x, 0)$, where f_d is a dynamic coefficient of friction. A typical value of the static coefficient of friction for rock is $f_s = 0.6$. As discussed by RSP, there is less certainty about appropriate values of f_d, but they suggest ratios f_d/f_s in the range 0.2 to 0.8 with a preference for the lower end of the range. Slip continues at constant stress τ_r until the trailing edge of the slip zone at $x = -L$. No further slip accumulates for $x \le -L$ and stress increases above τ_r. RSP assume a linear decrease of shear stress from τ_p to τ_r with distance behind the leading edge of the slip zone. If $L \to \infty$, the model reduces to the semi-infinite slip zone considered by *Poliakov et al.* [2002]. As discussed by RSP, when the slip zone is much larger than the end zone size, $L \gg R$, as in the *Poliakov et al.* [2002] model, the initial stress σ^0_{xy} is not significantly different from the residual friction stress τ_r.

[7] Because the fault is fluid saturated, and we are interested in changes relative to the ambient state of stress σ^0_{ij} and pore pressure p^0 before rupture, we will write $\bar{\sigma}_{yy}(x, 0)$ in (2) as $\sigma_{yy}(x, 0) + \Delta p$ where Δp is the change in pore pressure from the ambient value; this reinterprets $\sigma_{yy}(x, 0)$ as the ambient effective normal stress $\sigma^0_{yy} + p^0$; the reinterpreted term $\sigma_{yy}(x, 0)$, written σ_{yy} for shortness subsequently, is constant during the rupture. Our goal is to calculate the effect of the pressure induced by dynamic propagation on the frictional resistance. In order to make the problem simply tractable, we assume that the weakening from τ_p to τ_r is unaffected by changes in effective normal stress, as if it represented a true shear cohesion that was weakened by slip and ultimately lost. The part of the strength normally denoted by τ_r is wholly frictional in origin and is directly proportional to effective normal stress. Hence this part of the strength is variable along the fault. Thus we assume

$$\tau = \tau^0(x) - f_r\Delta p \quad (3)$$

where f_r is a constant and now $\tau_r = -f_r\sigma_{yy}(x, 0)$ in (1). Effectively, then, we are considering a strength relation in the form

$$\tau = c(\delta) - f_r\left(\sigma_{yy} + p\right) \quad (4)$$

where $c(\delta)$ is the cohesive part of strength, assumed to weaken with slip δ. For simplicity, the particular function

$c = c(\delta)$ is chosen to make $c(\delta)$ vary linearly with x, from $c(0)$ at the rupture tip $x = 0$ to 0 at $x = -R$. In that interpretation, $\tau_p - \tau_r$ is simply to be regarded as a way of writing $c(0)$.

[8] During dynamic slip propagation, there is insufficient time for pore fluid diffusion and conditions are undrained except for the small but critical boundary layer effect along the fault walls that is addressed in Appendix B. This effect takes place over a spatial scale perpendicular to the fault that is typically on the order of a few millimeters to a few tens of millimeters. When the slip surface is idealized as a completely impermeable plane, undrained conditions pertain right up to the surface itself and the change in pore pressure is related to total stress changes $\Delta\sigma_{ij}$ by

$$\Delta p = -\frac{1}{3}B\left(\Delta\sigma_{xx} + \Delta\sigma_{yy} + \Delta\sigma_{zz}\right) \tag{5}$$

where B is Skempton's coefficient. In an infinite, isotropic and homogeneous linear elastic solid, slip on a straight, planar fault induces no change in the normal stress on the fault plane and, consequently, $\Delta\sigma_{yy}$ vanishes on $y = 0$. For plane strain, the change of the out-of-plane normal stress is given there by $\Delta\sigma_{zz} = \nu_u\Delta\sigma_{xx}$ where ν_u is the undrained Poisson's ratio. Thus the change in pore pressure is

$$\Delta p(x, 0^+) = -\frac{1}{3}B(1 + \nu_u)\Delta\sigma_{xx}(x, 0^+) \tag{6}$$

where the superscript plus indicates evaluation on $y = 0$ as it is approached through positive values. For right-lateral slip, the pore pressure will increase on the positive side of the x axis. Substituting (6) into (3) and subtracting the initial, ambient shear stress σ^0_{xy} yield the change in shear stress on the plus side of the slip plane as

$$\Delta\sigma_{xy}(x, 0^+) = \frac{1}{3}f_rB(1 + \nu_u)\Delta\sigma_{xx}(x, 0^+) + g(x) \tag{7}$$

where

$$g(x) = \tau^0(x) - \sigma^0_{xy} = \begin{cases} -\left(\sigma^0_{xy} - \tau_r\right) + \left(\tau_p - \tau_r\right)(1 + x/R), & -R \le x < 0 \\ -\left(\sigma^0_{xy} - \tau_r\right), & -L \le x < -R \end{cases} \tag{8}$$

[9] In Appendix B, we show that the more elaborate model of the near fault material leads to an expression for the change in pore pressure that is identical to (6) but with B replaced by $B' = BW/w$, where B is now to be interpreted as the Skempton coefficient outside the near fault border regions (as ν_u is the undrained Poisson's ratio of this region) and w and W (given in Appendix B) depend on the poroelastic properties and permeabilities of the near fault materials to either side (inset of Figure 1). Thus, in all the following expressions, B is replaced by B'. Because W may be either positive or negative, the pore pressure may increase, promoting slip by decreasing the effective compressive normal stress, or decrease, inhibiting slip by increasing the effective compressive normal stress. If the only alteration of the effective normal stress is the pore pressure induced by the near slip plane dissimilarity of properties, then it is reasonable to assume, as did *Rudnicki and Koutsibelas* [1991], that the pore pressure increase controls propagation. However, this effect is likely to act in combination with others, such as that due to elastic dissimilarity of material farther from the fault discussed in the next paragraph. Consequently, we will present results for near slip zone arrangement of properties that both increase and decrease pore pressure.

[10] If the materials away from the near fault region are modeled as elastic, but with different properties on the two sides of the fault, then inhomogeneous slip at the interface induces a change in normal stress *Comninou* [1978] and *Adams* [1995, 1998] in addition to the change in effective normal stress caused by the pore pressure (i.e., $\Delta\sigma_{yy} \neq 0$ on $y = 0$, as assumed above). This change may also be positive or negative depending on the direction of slip, the direction of propagation and the mismatch of properties. In a later section, we compare the alteration of normal stress in this case to the alteration of effective normal stress due to pore pressure and show that the net change in effective normal stress is the combination of both effects.

[11] We also note that neglecting pore pressure effects but assuming a linear dependence of the friction coefficient, or simply of the shear strength, on the slip rate $\dot{\delta}$ leads to a linear relation of the same form as (7) between the changes in shear stress $\Delta\sigma_{xy}(x, 0^+)$ and the fault parallel stress change $\Delta\sigma_{xx}(x, 0^+)$ on the fault plane. This follows from the connection between the slip rate and the fault parallel normal strain for steady propagation (see (B1) and the following parenthetical remark). Although we do not treat this case, the solution could be obtained from that here. In particular, for a friction coefficient of the form $f_r = f_r^0 + f_r^1\dot{\delta}$, equations in the same form as equations (7) and (8) hold, but now with $\tau_r = -f_r^0\sigma_{yy}$ and with $f_rB(1 + \nu)/3$ in equation (7) replaced by $f_r^1\mathrm{v}(1 - \nu)\sigma^0_{yy}/\mu$. (An analogous solution with velocity strengthening friction has been developed recently by *Brener et al.* [2005] for self-healing slip pulses at a nonopening interface between deformable and rigid solids.)

3. Solution

[12] RSP have shown that the change in total stresses for steady propagation of a Mode II rupture can be written as follows in terms of a single analytic function $M(z)$ of the complex variable z

$$\Delta\sigma_{xx} = \Delta\bar{\sigma}_{xx} - \Delta p = 2\alpha_s\mathrm{Im}\left[\left(1 - \alpha_s^2 + 2\alpha_d^2\right)M(z_d) - \left(1 + \alpha_s^2\right)M(z_s)\right]/D \tag{9a}$$

$$\Delta\sigma_{yy} = \Delta\bar{\sigma}_{yy} - \Delta p = -2\alpha_s\left(1 + \alpha_s^2\right)\mathrm{Im}[M(z_d) - M(z_s)]/D \tag{9b}$$

$$\Delta\sigma_{xy} = \Delta\bar{\sigma}_{xy} = \mathrm{Re}\left[4\alpha_s\alpha_dM(z_d) - \left(1 + \alpha_s^2\right)^2M(z_s)\right]/D \tag{9c}$$

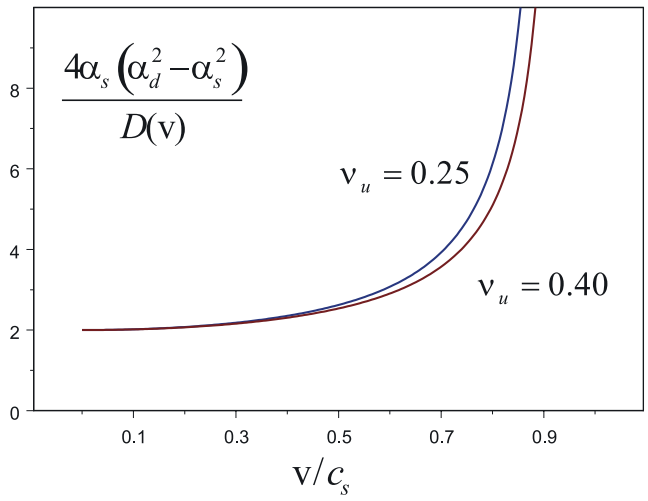

Figure 3. Velocity-dependent portion of k (first bracket in (13)) against the rupture velocity v divided by the shear wave speed c_s for two values of the undrained Poisson's ratio, 0.25 and 0.40.

where $z_d = x + i\alpha_d y$, $z_s = x + i\alpha_s y$, $\alpha_d = \sqrt{1-(\mathrm{v}/c_d)^2}$, $\alpha_s = \sqrt{1-(\mathrm{v}/c_s)^2}$, c_d and c_s are the dilatational and shear wave speeds, and Re and Im stand for the real and imaginary parts. The denominator is the Rayleigh function

$$D = 4\alpha_s\alpha_d - \left(1+\alpha_s^2\right)^2 \tag{10}$$

which vanishes when v equals the Rayleigh wave speed. (RSP used the notation σ_{ij}^{tot} for what we call the total stress σ_{ij} here, and used the notation σ_{ij} for what we call the effective stress $\bar{\sigma}_{ij}$ here.)

[13] Evaluating (9a) and (9c) on the slip plane $y = 0$ yields

$$\Delta\sigma_{xx}\left(x,0^{\pm}\right) = \frac{4\alpha_s\left(\alpha_d^2-\alpha_s^2\right)}{D}\mathrm{Im}\left[M^{\pm}(x)\right] \tag{11a}$$

$$\Delta\sigma_{xy}\left(x,0^{\pm}\right) = \mathrm{Re}\left[M^{\pm}(x)\right] \tag{11b}$$

where the superscript plus or minus indicates the limit as $y = 0$ is approached through positive or negative values. Substituting into (7) then gives

$$\mathrm{Re}[M^+(x)] = k\mathrm{Im}[M^+(x)] + g(x) \text{ on } -L \le x \le 0 \tag{12}$$

where, using equation (6) with B' replacing B, as discussed following equation (8)

$$k = f_r\left[\frac{4\alpha_s\left(\alpha_d^2-\alpha_s^2\right)}{D}\right]\left[\frac{B'(1+\nu_u)}{3}\right] \tag{13}$$

[14] Because the shear stress is continuous on the entire plane $y = 0$ (including the slipping region), the same arguments used by RSP can be used to show that $M(z) = \bar{M}(z)$, where $\bar{M}(z)$ is defined by $\bar{M}(z) = \overline{M(\bar{z})}$ and the overbar denotes the complex conjugate. As a consequence, the real and imaginary parts of $M^+(x)$ in (12) can be written as

$$2\mathrm{Re}[M^+(x)] = M^+(x) + M^-(x) \tag{14a}$$

$$2i\mathrm{Im}[M^+(x)] = M^+(x) - M^-(x) \tag{14b}$$

Substituting these into (12) and rearranging give

$$(1+ki)M^+(x) + (1-ki)M^-(x) = 2g(x) \text{ on } -L \le x \le 0 \tag{15}$$

The problem has been reduced to finding the function $M(z)$ that is analytic everywhere in the cut plane and approaches values on either side of the cut $-L \le x \le 0$ that are related by (15) with (8). This is a type of problem that arises commonly in complex variable formulations of elasticity. Detailed discussions are given by *Muskhelishvili* [1992] and *England* [2003]. The solution is obtained by a modified version of the procedure used by RSP and is described in Appendix A. Results for a mathematically similar problem arising in supershear rupture propagation are given in the auxiliary material of *Dunham and Archuleta* [2005].

[15] The desired function is

$$M(z) = -\left(\sigma_{xy}^0 - \tau_r\right) - \left(\tau_p - \tau_r\right)\frac{\cos(\pi\varepsilon)}{\pi}z^{\frac{1}{2}-\varepsilon}(z+L)^{\frac{1}{2}+\varepsilon} \cdot \int_{-R}^{0}\frac{(1+t/R)dt}{(-t)^{\frac{1}{2}-\varepsilon}(t+L)^{\frac{1}{2}+\varepsilon}(t-z)} \tag{16}$$

where ε is given by

$$\varepsilon = \frac{1}{\pi}\arctan(k) \tag{17}$$

When $\varepsilon = 0$ (which occurs for $B = B' = 0$) the expression for $M(z)$ reduces to that of RSP. Because $D = 0$ (see (13)) when the rupture speed v equals the Rayleigh wave velocity ($\approx 0.92\ c_s$ when $\nu_u = 0.25$ and $0.94\ c_s$ for $\nu_u = 0.4$), in this limit k becomes unbounded and $\varepsilon = \pm 1/2$, depending on the sign of B'. (Recall that for $B' < 0$ the extended side of the fault is more permeable than the compressed side.) At v = 0, the first bracket in (13) equals 2. Thus both k and ε have finite values at zero velocity and the effects of the pore pressure persist at low velocities, if not so low that the description of the field as being undrained almost everywhere loses validity. Figure 3 plots the velocity-dependent portion of k (first bracket in (13)) against the rupture speed v divided by the shear wave speed c_s for two values of the undrained Poisson's ratio $\nu_u = 0.25$ and 0.40. The second bracket vanishes if the fluid is very compressible ($B = B' = 0$) and is equal to one half in the limit of incompressible solid and fluid constituents for a homogeneous material ($B = B' = 1$ and $\nu_u = 1/2$). Thus, for the latter limit and zero velocity k is simply equal to f_r.

[16] Figure 4 shows the variation of ε with v/c_s for three values of the friction coefficient (0.6, 0.4, and 0.2) and two values of the effective Skempton coefficient B' (0.9 and 0.5) for $\nu_u = 0.4$. If $B' < 0$, the values of ε are the negative of those shown. Since the decrease of the friction coefficient from a static to a dynamic value is neglected in the portion

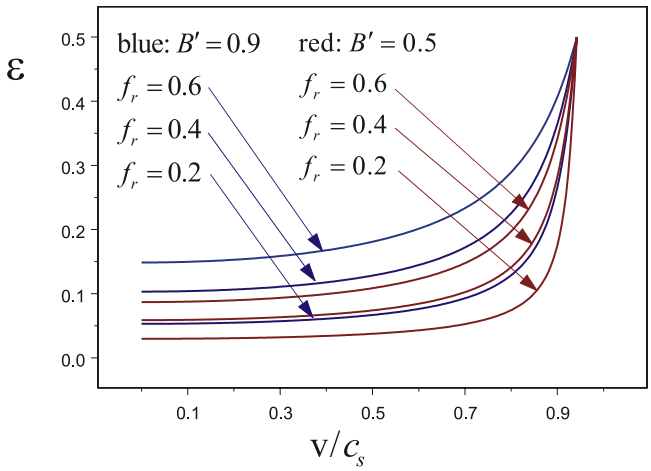

Figure 4. Variation of ε with v/c_s for undrained Poisson's ratio $\nu_u = 0.4$, three values of the friction coefficient and two values of the effective Skempton coefficient B'.

multiplying the pore pressure (3) or is regarded as a separate cohesive term (4), the appropriate value of f_r should lie between the static and dynamic values and, likely, closer to the dynamic (residual) value. The higher value of B' might be more appropriate for a highly comminuted and disaggregated fault zone that is much more permeable on the compressive side. However, as discussed in the Appendix B, a smaller contrast in permeability and a lower shear modulus for the near fault material on the compressive side (relative to the modulus for the less damaged material farther away) tends to reduce the effective value of Skempton's coefficient. This reduction is reflected by the choice of $B' = 0.5$. Figure 3 shows that the velocity-dependent portion of k (and ε) does not depend strongly on ν_u and otherwise ν_u enters only as a product with B' in the sum $1 + \nu_u$.

4. Pore Pressure

[17] Combining (6) and (11a) and using the expression for k (13) give the change of pore pressure on the positive side of the y axis

$$f_r \Delta p(x, 0^+) = -k \mathrm{Im}\{M^+(x)\} \tag{18}$$

where $\mathrm{Im}\{M^+(x)\}$ is the imaginary part of $M(z)$ as y approaches zero through positive values in $-L \le x \le 0$. This can be calculated numerically directly from (16) but is also given by (A8) of the Appendix A. Pore pressure changes for positive and negative values of ε with magnitudes equal to 0.1, 0.2, 0.3, 0.4, and 0.45 are plotted for $L/R = 2.0$ and $L/R = 5.0$ in Figure 5.

[18] For the six cases plotted in Figure 4, the magnitude of ε at zero velocity ranges from a few per cent (0.03 for $B' = 0.5$ and $f_r = 0.2$) to 0.15 for $B' = 0.9$ and $f_r = 0.6$. For $B' = 0.9$, $\varepsilon = 0.2$ corresponds to v/c_s equal to 0.59, 0.76 and 0.87 for $f_r = 0.6$, 0.4 and 0.2, respectively; for $B' = 0.5$, $\varepsilon = 0.2$ corresponds to v/c_s equal to 0.80, 0.86 and 0.891 for $f_r = 0.6$, 0.4 and 0.2, respectively. A magnitude of $\varepsilon = 0.3$ corresponds to rupture speeds of $0.81c_s$, $0.87c_s$, $0.91c_s$, $0.88c_s$, $0.916c_s$ and $0.93c_s$ for the six cases plotted in Figure 4. Magnitudes of ε equal to 0.4 and 0.45 correspond to rupture speeds ranging from $0.90c_s$ (for $B' = 0.9$, $f_r = 0.6$) to $0.94c_s$ (nearly the Rayleigh wave speed $c_r = 0.94c_s$ for $\nu_u = 0.4$) for the parameters used in Figure 4.

[19] For positive values of ε, the pore pressure increases rapidly at the onset of slip at $x = 0$ and the largest pore pressure increase is induced in the end zone near the front of the slipping zone. The magnitude of the induced pressure increases with ε and $f_r \Delta p(x, 0^+)$ can exceed 80% of

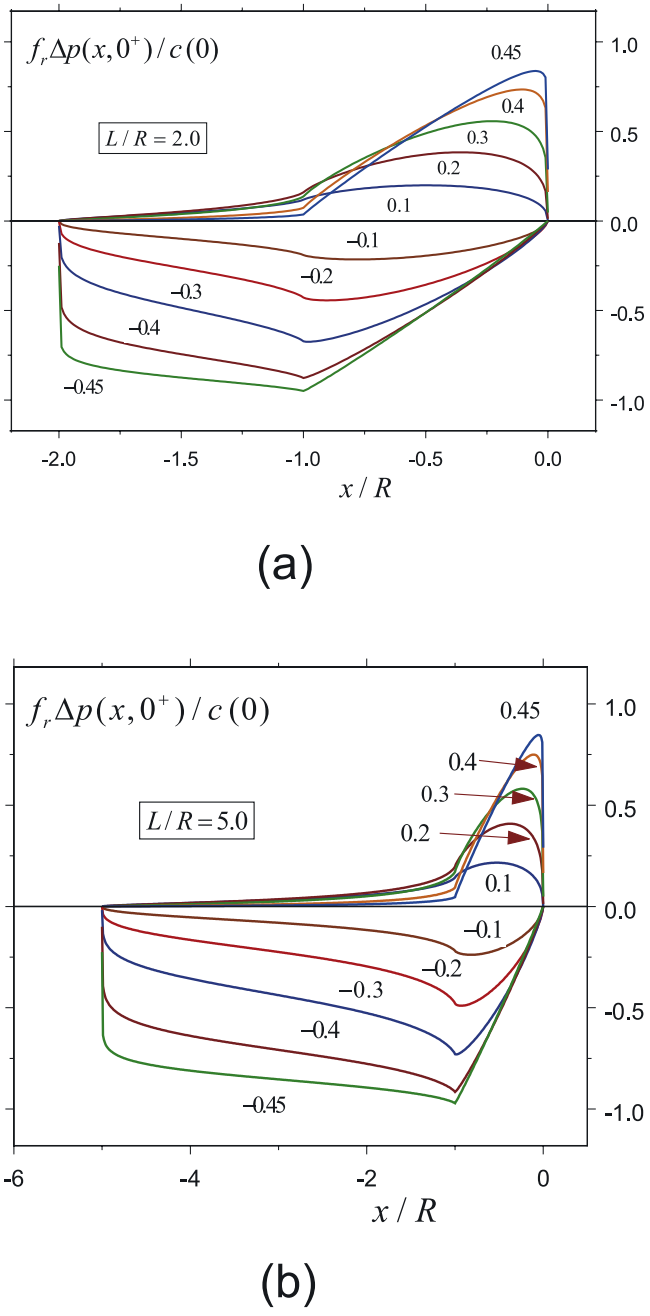

Figure 5. Induced pore pressure $\Delta p(x, 0^+)$ multiplied by the friction coefficient f_r and divided by the cohesive zone stress drop $c(0) = \tau_p - \tau_r$. Results are shown for (a) $L/R = 2.0$ and (b) for $L/R = 5.0$. Curves are labeled by positive and negative values of ε for five magnitudes: 0.1, 0.2, 0.3, 0.4, and 0.45.

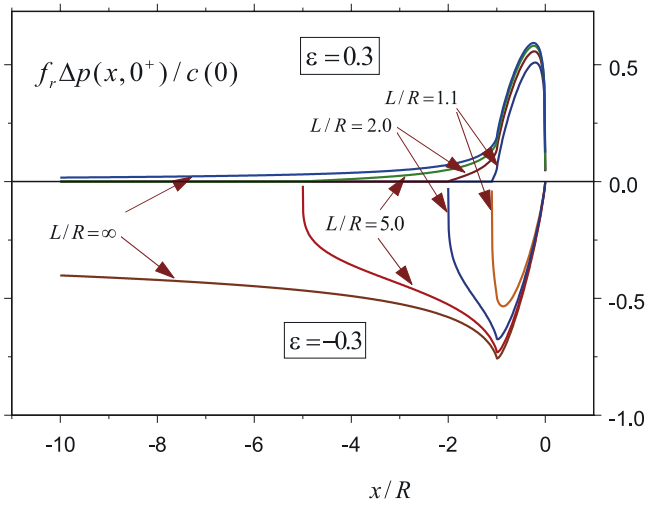

Figure 6. Dependence of the pore pressure changes on L/R. Results are shown for $\varepsilon = \pm 0.3$ and $L/R = 1.1$, 2.0, 5.0 and the limit $L/R \rightarrow \infty$.

$c(0) = \tau_p - \tau_r$ for $\varepsilon = 0.45$. Since ε increases with increasing velocity, the induced pore pressure contributes to velocity weakening. The distribution of pore pressure is more sharply peaked in the end zone for the larger values of ε. For negative values of ε, the pore pressure decreases roughly linearly with the onset of slip at $x = 0$ and achieves its largest decrease near the end of the slip weakening zone ($x = -R$). As for positive ε, the magnitude of the change increases with the magnitude of ε and $f_r\Delta p(x, 0^+)$ is about 95% of $\tau_p - \tau_r$ for $\varepsilon = -0.45$. Because increasing magnitude of ε corresponds to increasing velocity, the increasing magnitude of the pore pressure decrease (increasing effective compressive stress) inhibits rupture propagation.

[20] The maximum induced pore pressure depends weakly on L/R and is about the same in Figures 5a and 5b. This is shown more clearly in Figure 6, which plots the induced pore pressure $f_r\Delta p$ (divided by $c(0) = \tau_p - \tau_r$) for $\varepsilon = \pm 0.3$ and $L/R = 1.1$, 2.0, 5.0 and the limit $L/R \rightarrow \infty$. The magnitude of the pore pressure change induced in the end zone increases only slightly with L/R.

[21] The magnitudes of the pore pressure changes induced outside the end zone ($-L \leq x < -R$) differ significantly for positive and negative values of ε. For $\varepsilon > 0$, a pore pressure increase with a magnitude roughly 10 to 20% of $\tau_p - \tau_r$ is induced on the slipping zone outside the end zone. The magnitude is slightly larger and the decay toward the end of the slip zone ($x = -L$) is slower for the smaller values of ε. Figure 6 shows that the magnitude of the pore pressure induced outside the end zone, although a small fraction of $\tau_p - \tau_r$, increases with increasing L/R. The pore pressure increase induced on $-L < x < -R$ reduces the effective value of the residual friction stress. For a maximum magnitude of $f_r\Delta p$ outside the end zone about 20% of $\tau_p - \tau_r$ and the range of $\tau_r/\tau_p = 0.2$–0.8 (corresponding to the range of the ratio of static to dynamic values of the friction coefficient f_s/f_d cited earlier from RSP), $f_r\Delta p$ ranges from 0.05 to 0.80 times τ_r. Thus the effective frictional resistance remains positive although it can be reduced to as little as 20% of its nominal value.

[22] For $\varepsilon < 0$, the magnitude of the pore pressure decreases slowly from its largest value near the end of the weakening zone ($x = -R$) until very close to the trailing edge of the slip zone where it drops abruptly to zero. (The different behaviors of the pore pressure at the leading and trailing edges for positive and negative ε are evident from the effects on the exponents of $-x$ and $L + x$ in (A8)). Thus the pore pressure decrease increases the effective value of the frictional resistance by a substantial fraction of $\tau_p - \tau_r$ for the larger magnitudes of ε. For negative ε, the magnitude of the pore pressure change is greater over a larger proportion of the slipping zone. Figure 6 shows that the effect is more dramatic for larger L/R.

[23] The induced pore pressure alters the effective shear resistance, $\tau^0(x) - f_r\Delta p(x, 0^+)$, and changes its distribution on the slip zone. The effective shear resistance minus the residual resistance τ_r (divided by $\tau_p - \tau_r$) is shown for the same values of ε in Figure 7 for $L/R = 2.0$ and 5.0. For comparison the nominal, linear distribution of shear resistance in the absence of pore pressure change, $\tau^0(x)$, minus τ_r, is also plotted. As shown, for $\varepsilon > 0$, the induced pore pressure increase causes a much more precipitous drop in the shear resistance with distance back from the edge of the slipping zone ($x = 0$). As already noted, the pore pressure causes a reduction in the effective residual shear resistance on the slipping region outside the end zone (negative values in Figure 7 for $-L \leq x < -R$). For $\varepsilon < 0$, the pore pressure decrease causes a more gradual decrease in the shear resistance until very near the trailing edge of the slip zone and causes the shear resistance to remain closer to τ_p over the entire slipping region (rather than dropping to τ_r). For both positive and negative ε, the effect is larger for larger magnitudes and hence larger velocities. For negative ε, the effective residual shear resistance is increased much more than it is decreased for positive ε.

5. Energy Release Rate

[24] In this section, we calculate and discuss the effect of the induced pore pressure on the energy required to drive the fault at given a velocity (for a given nominal slip weakening relation). For steady state propagation of the slip zone, there can be no change in the strain energy or kinetic energy. Consequently, as noted by RSP, the work of the applied stress on the total relative slip must equal the energy dissipated against the frictional resistance

$$\sigma^0_{xy}\delta_T = \int_0^{\delta_T} \left[\tau^0(\delta) - f_r\Delta p\right] d\delta \tag{19}$$

where $\delta_T = \delta(x = -L)$ is the total relative displacement accumulated at the trailing edge of the slipping zone and τ^0 is regarded as a function of slip accumulated behind the tip δ rather than position x (see section 6). Using $\Delta\sigma_{yy} = 0$, subtracting $\tau_r\delta_T$ from both sides, and noting that $\tau^0 - \tau_r = 0$ for $\delta(x = -R) \leq \delta \leq \delta_T$ gives

$$\left(\sigma^0_{xy} - \tau_r\right)\delta_T = \int_0^{\delta(x=-R)} \left[\tau^0(\delta) - \tau_r\right] d\delta - f_r \int_0^{\delta_T} \Delta p d\delta \tag{20}$$

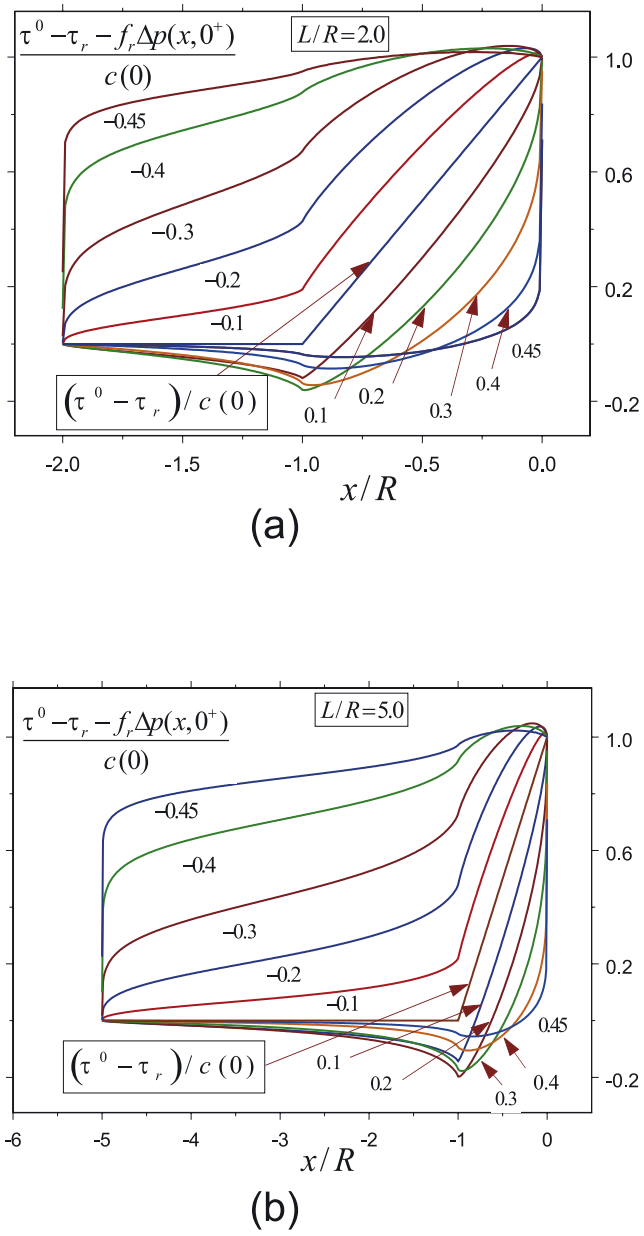

Figure 7. Effective frictional resistance minus τ_r (divided by $c(0) = \tau_p - \tau_r$) for (a) $L/R = 2.0$ and (b) $L/R = 5.0$. Curves are labeled by positive and negative values of ε. Also shown is the nominal slip weakening in the absence of pore pressure changes τ^0.

[25] The left side of (20) is the nominal energy supplied by the applied loads in excess of the work against the residual friction stress τ_r:

$$\mathcal{G}_{\text{nom}} = \frac{\left(\sigma^0_{xy} - \tau_r\right)}{\left(\tau_p - \tau_r\right)}\left(\tau_p - \tau_r\right)\delta_T \tag{21}$$

where we have divided and multiplied by $(\tau_p - \tau_r)$. In Appendix A, we show that the scaled stress drop ratio can be written as

$$\frac{\sigma^0_{xy} - \tau_r}{\tau_p - \tau_r} = \frac{\cos(\pi\varepsilon)}{\pi}\left(\frac{R}{L}\right)^{\frac{1}{2}+\varepsilon}\Sigma\left(\frac{R}{L};\varepsilon\right) \tag{22}$$

where

$$\Sigma\left(\frac{R}{L};\varepsilon\right) = \int_0^1 \frac{(1-p)}{p^{\frac{1}{2}-\varepsilon}[1-(R/L)p]^{\frac{1}{2}+\varepsilon}}dp \tag{23}$$

When $\varepsilon = 0$, the integral can be solved exactly to give the result in RSP and in the limit $R/L \to 0$, $\Sigma(0;\varepsilon) = 1/[(1/2+\varepsilon)(3/2+\varepsilon)]$. Figure 8 plots (22) with (23) for various values of ε. For a fixed value of R/L and positive ε, the induced pore pressure increase reduces the driving stress $\sigma^0_{xy} - \tau_r$ for a given cohesive zone stress drop; for negative ε the induced reduction of pore pressure increases the driving stress.

[26] In the Appendix A, we also show that the total locked-in displacement can be expressed as

$$\delta_T = \frac{2(\tau_p - \tau_r)\cos(\pi\varepsilon)}{\mu F(\text{v})}L\left(\frac{R}{L}\right)^{\frac{1}{2}+\varepsilon}\Delta\left(\frac{R}{L};\varepsilon\right) \tag{24}$$

where $F(\text{v}) = D(\text{v})/\alpha_s(1-\alpha_s^2)$ as in RSP and

$$\Delta\left(\frac{R}{L};\varepsilon\right) = \int_0^1 \frac{(1-p)[(1/2+\varepsilon)-(R/L)p]}{p^{\frac{1}{2}-\varepsilon}[1-(R/L)p]^{\frac{1}{2}+\varepsilon}}dp \tag{25}$$

In the limit $R/L \to 0$, $\Delta(0;\varepsilon) = 1/(1/2+\varepsilon)$. When $\varepsilon = 0$, the integral can be solved exactly to give the result in RSP and when v approaches the Rayleigh wave speed so that $\varepsilon = 1/2$, $\Delta(R/L;1/2) = 1/2$. Substituting for the stress ratio from (22) and for δ_T from (24) gives the following expression for $\mathcal{G}_{\text{nom}}$:

$$\mathcal{G}_{\text{nom}} = \frac{2}{\pi}\frac{\left[(\tau_p - \tau_r)\cos(\pi\varepsilon)\right]^2}{\mu F(\text{v})}L\left(\frac{R}{L}\right)^{1+2\varepsilon}\Delta(R/L;\varepsilon)\Sigma(R/L;\varepsilon) \tag{26}$$

$\mathcal{G}_{\text{nom}}$ reduces to RSP (their equation (18)) for $\varepsilon = 0$ and in the limit $R/L \to 0$, $\mathcal{G}_{\text{nom}}/(\mu\delta_T^2/\pi L)$ reduces to $F(\text{v})/(1+\varepsilon)$ which also agrees with RSP for $\varepsilon = 0$.

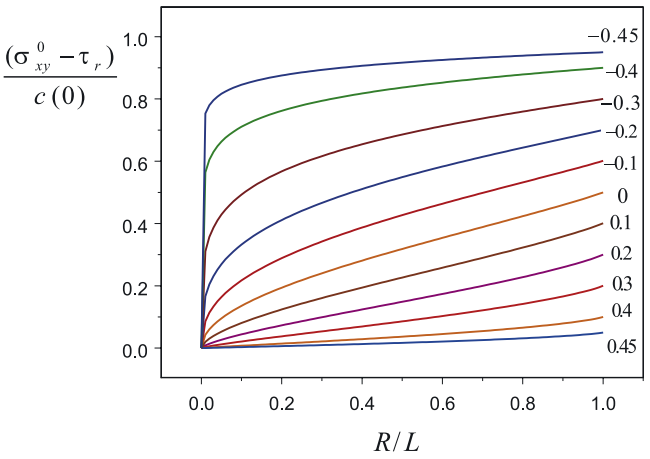

Figure 8. Stress drop scaled by the cohesive stress drop $c(0) = \tau_p - \tau_r$ against R/L for various values of ε (values to the right of the curves).

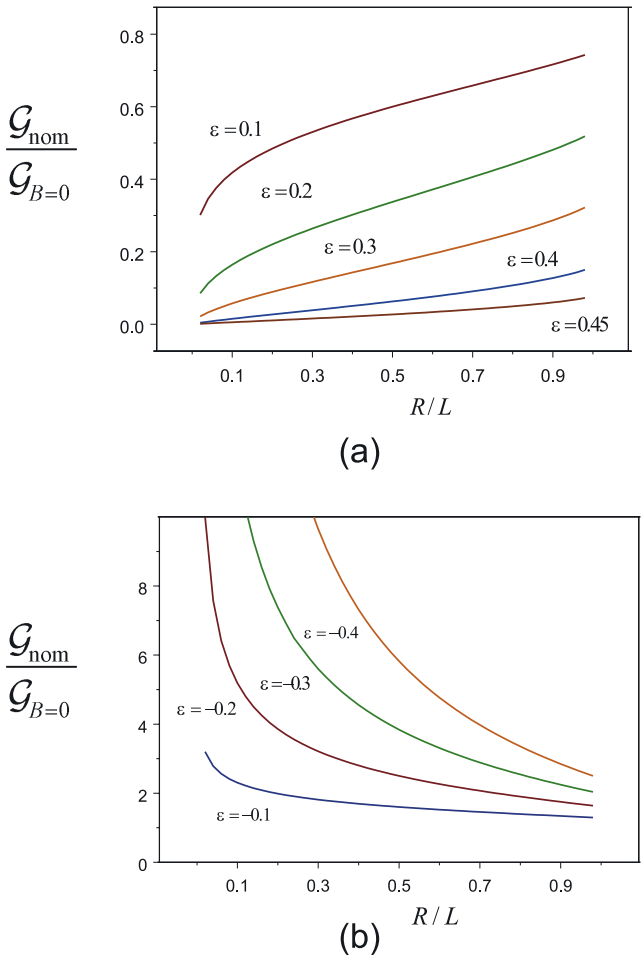

Figure 9. Nominal energy supplied by the applied loads $\mathcal{G}_{nom}$ divided by the material value in the absence of porous media effects $\mathcal{G}_{B=0}$ against R/L for (a) five positive values of the velocity-dependent parameter ε = 0.1, 0.2, 0.3, 0.4 and 0.45 and (b) four negative values −0.1, −0.2, −0.3, and −0.4.

[27] In the absence of induced pore pressure or when the Skempton coefficient, B, is zero, $\mathcal{G}_{nom}$ is equal to the energy dissipated against friction in excess of τ_r in the end zone, $-R \le x \le 0$, which is the first term on the right in (20):

$$\mathcal{G}_{B=0} = \int_0^{\delta(x=-R)} \left(\tau^0(\delta) - \tau_r\right) d\delta \tag{27}$$

Within the idealization here that τ^0 is unaffected by the pore pressure, we regard $\mathcal{G}_{B=0}$ as a material parameter. For the alternative interpretation of the slip weakening as purely cohesive, expressed by (4),

$$\mathcal{G}_{B=0} = \int_0^{\delta(x=-R)} c(\delta) d\delta \tag{28}$$

with $c(\delta) = 0$ for $\delta \ge \delta(x = -R)$. Thus, for a given value of $\mathcal{G}_{B=0}$, reflecting a given τ versus δ relation in the end zone (in the absence of pore pressure), the effect of an increase in pore pressure is to reduce the energy that must be supplied to drive the fault. Conversely, a decrease in pore pressure increases the energy that must be supplied.

[28] Using $d\delta = (\partial\delta/\partial x)dx$ and changing the limits of integration in the second term on the right in (20) yield

$$\mathcal{G}_{nom} = \mathcal{G}_{B=0} - f_r \int_0^{-L} \Delta p(x, 0^+) \frac{\partial \delta}{\partial x}(x) dx \tag{29}$$

Substituting for $\Delta p(x, 0^+)$ from (18), for $\partial\delta/\partial x$ from (A13) and then from (A15) gives

$$\mathcal{G}_{nom} = \mathcal{G}_{B=0} - \frac{2kL}{\mu F(\mathrm{v})} \left[\frac{1}{\pi}\left(\tau_p - \tau_r\right)\cos(\pi\varepsilon)\right]^2 \cdot \int_0^1 \left[H\left(-\xi\frac{L}{R}; \frac{R}{L}\right)\right]^2 d\xi \tag{30}$$

where we have used the change of variable $\xi = -x/L$ in the integral. Thus the second term on the right side gives the amount that the nominal energy needed to drive the fault for a fixed material fracture energy ($\mathcal{G}_{B=0}$) is reduced by an induced pore pressure increase (ε, $k > 0$) or increased by a pore pressure decrease (ε, $k < 0$). Dividing by $\mathcal{G}_{B=0}$ and using (26) give the ratio

$$\frac{\mathcal{G}_{nom}}{\mathcal{G}_{B=0}} = \frac{1}{1 + X} \tag{31}$$

where

$$X = \frac{k \int_0^1 \left[H\left(\frac{L}{R}\xi; \frac{R}{L}\right)\right]^2 d\xi}{\pi (R/L)^{1+2\varepsilon} \Delta(R/L; \varepsilon) \Sigma(R/L; \varepsilon)} \tag{32}$$

This ratio is unity in the absence of pore fluid effects ($B = 0$) and thus for positive ε gives the fraction by which the energy that must be supplied to drive the fault is reduced; for negative ε the ratio exceeds unity and gives the proportion by which the energy must be increased.

[29] Figure 9 plots (31) as a function of R/L for positive (Figure 9a) and negative (Figure 9b) values of ε. Thus, for $\varepsilon > 0$, the energy that must be supplied to drive the fault decreases with ε and increasing propagation velocity. Recall that for the values of B, and f_r used in Figure 4, the magnitude of ε at zero velocity ranges from a few per cent to 0.15. A magnitude of ε = 0.3 corresponds to rupture speeds of $0.81c_s$, $0.87c_s$, $0.91c_s$, $0.88c_s$, $0.916c_s$ and $0.93c_s$ for the six cases plotted in Figure 4. Magnitudes of ε equal to 0.4 and 0.45 correspond to rupture speeds ranging from $0.90c_s$ to $0.94c_s$ (nearly the Rayleigh wave speed $c_r = 0.94c_s$ for $\nu_u = 0.4$) for the parameters used in Figure 4. Consequently, the reduction is substantial, and is more than 50%, for rupture speeds in excess of about $0.5c_s$.

[30] There is an increase in (31) with R/L, which is greater for smaller values of ε. Since the peak induced pore pressure depends only weakly on R/L, this increase reflects the more rapid decline in pore pressure outside the end zone for the larger values of R/L (see Figure 6).

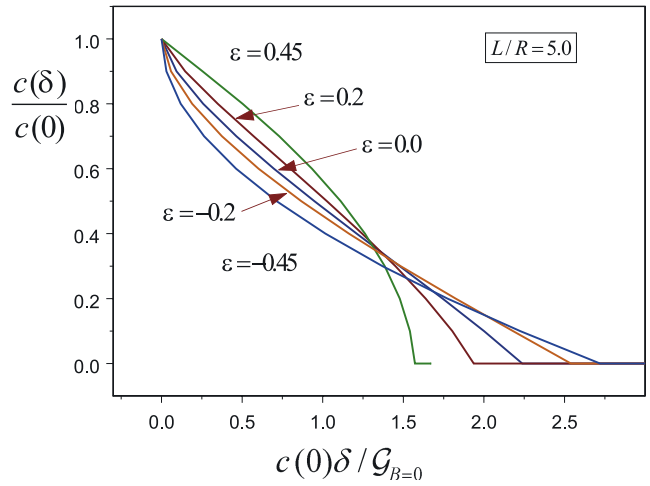

Figure 10. Relation for the cohesive part of the stress drop $c(\delta)$, divided by $c(0) = \tau_p - \tau_r$, versus relative slip, multiplied by $c(0)/\mathcal{G}_{B=0}$, implied by the solution. Shown for $L/R = 5.0$ and several values of ε.

[31] For negative values of ε, the reduction in pore pressure dramatically increases the energy needed to drive the fault, by ratios exceeding 2, except when the slip weakening zone is a large fraction of the total slip zone length ($R \approx L$). For fixed R/L, the energy required increases with velocity and hence would tend to inhibit propagation. The very large increases in energy required for small R/L reflect the large decreases in pore pressure induced outside the end zone ($-L \le x \le -R$) as shown in Figures 5 and 6.

6. Implied Slip Weakening Law

[32] The frictional shear stress $\tau^0(x)$ in the absence of pore pressure has been assumed to decrease linearly with distance behind the rupture edge as shown schematically in Figure 2. Because the resulting relative displacements on the slip zone can be calculated, as noted by RSP (following *Palmer and Rice* [1973]), the distribution of $\tau^0(x)$ implies a relation between τ^0 and the slip δ. In the absence of induced pore pressure, this relation is independent of rupture speed. Although the relation is not linear and depends on R/L, RSP show (by comparing results for the limiting cases of $R/L = 0$ and $R/L = 1$) that the departure from linearity is small and that the dependence on R/L is weak for a fixed material fracture energy (their G and corresponding to our $\mathcal{G}_{B=0}$).

[33] In contrast to RSP, the slip weakening relation here depends on the rupture velocity (and porous media parameters) through ε. Figure 10 shows the effective shear resistance against the relative slip (multiplied by $c(0)/\mathcal{G}_{B=0}$) for $L/R = 5.0$ and $\varepsilon = \pm 0.2$ and ± 0.45. The relation is also plotted for $\varepsilon = 0$, corresponding to $B = 0$ and the case considered by RSP. As shown the decrease (increase) in pore pressure for $\varepsilon < (>)0$ causes the curve to drop more (less) rapidly for small displacements. The areas under the curves are required to be identical (equal to one for the normalization used) by (27) and (28) because the nominal energy release rate (for $B = 0$) is interpreted as a material parameter. As in RSP, the dependence on L/R is very weak and plots for the other values of L/R used (1.1, 1.5, 2.0., and 10.0) are virtually indistinguishable from Figure 10.

7. More General Perspective on Material Dissimilarity Effects in Dynamic Rupture

[34] In this section we compare the alteration of effective normal stress, due to induced pore pressure on the fault plane, with the change in normal stress induced by spatially inhomogeneous, mode II sliding on a plane between elastic solids with different material properties [*Comninou*, 1978; *Adams*, 1995, 1998]. The latter effect has been studied extensively in seismology [*Weertman*, 1980; *Andrews and Ben-Zion*, 1997; *Harris and Day*, 1997; *Cochard and Rice*, 2000; *Ben-Zion*, 2001; *Xia et al.*, 2005]. In particular, we show how differences in poroelastic properties in thin layers along the fault (as in Figure 1 and in Appendix B) modify the interpretation of material dissimilarity as it has been considered thus far.

[35] We adopt the formulation of *Weertman* [1980] for steadily traveling slip distributions of form $\delta = \delta(x - \mathrm{v}t)$ on the interface between homogeneous elastic half-spaces to illustrate the effect. In that formulation, the shear and normal stresses are

$$\sigma_{xy}(x) = \sigma^0_{xy} - \frac{\bar{\mu}(\mathrm{v})}{\pi}\int_{-\infty}^{+\infty}\frac{d\delta(x')/dx'}{x-x'}dx' \tag{33}$$

$$\sigma_{yy}(x) = \sigma^0_{yy} - \mu^*(\mathrm{v})d\delta(x)/dx \tag{34}$$

The functions, labeled $\bar{\mu}(\mathrm{v})$ and $\mu^*(\mathrm{v})$ by Weertman, are defined in terms of his additional functions of rupture speed v

$$\alpha_i = \sqrt{1-\mathrm{v}^2/2c_{si}^2}, \beta_i = \sqrt{1-\mathrm{v}^2/c_{si}^2}, \gamma_i = \sqrt{1-\mathrm{v}^2/c_{di}^2} \tag{35}$$

with $i = 1$ or 2. Weertman's subscript 1 refers to the material in $y > 0$ (where we previously denoted the near-fault material by plus), and 2 refers to that in $y < 0$ (with near-fault material denoted minus above). The α here should not be confused with earlier uses of that symbol; β and γ correspond to α_s and α_d, respectively, as introduced earlier. In terms of those functions [*Weertman*, 1980], with misprint corrections by *Cochard and Rice* [2000], $\bar{\mu}(\mathrm{v})$ and $\mu^*(\mathrm{v})$ are

$$\bar{\mu} = \frac{2\mu_1\mu_2}{\Delta_1+\Delta_2}\left[\mu_1\gamma_2(1-\alpha_2^2)(\gamma_1\beta_1-\alpha_1^4) + \mu_2\gamma_1(1-\alpha_1^2)(\gamma_2\beta_2-\alpha_2^4)\right] \tag{36}$$

$$\mu^* = \frac{2\mu_1\mu_2}{\Delta_1+\Delta_2}\left[\mu_1(\gamma_1\beta_1-\alpha_1^4)(\gamma_2\beta_2-\alpha_2^2) - \mu_2(\gamma_2\beta_2-\alpha_2^4)(\gamma_1\beta_1-\alpha_1^2)\right] \tag{37}$$

where

$$\Delta_1 = \mu_1\mu_2\left[\left(1-\alpha_1^2\right)\left(1-\alpha_2^2\right)\gamma_2\beta_1+\left(\gamma_1\beta_1-\alpha_1^2\right)\left(\gamma_2\beta_2-\alpha_2^2\right)\right] + \mu_2^2\left(1-\gamma_1\beta_1\right)\left(\gamma_2\beta_2-\alpha_2^4\right) \quad (38)$$

$$\Delta_2 = \mu_1\mu_2\left[\left(1-\alpha_1^2\right)\left(1-\alpha_2^2\right)\gamma_1\beta_2+\left(\gamma_1\beta_1-\alpha_1^2\right)\left(\gamma_2\beta_2-\alpha_2^2\right)\right] + \mu_1^2\left(1-\gamma_2\beta_2\right)\left(\gamma_1\beta_1-\alpha_1^4\right) \quad (39)$$

In the references cited, $\Delta_1 + \Delta_2$ above is written simply as Δ, but both Δ_1 and Δ_2 are needed for the present purposes.

[36] When the two materials are identical, as in the treatment of the materials far from the fault in the earlier part of this paper, $\mu^\star = 0$ and

$$\bar{\mu}(v) = \frac{\mu(\gamma\beta-\alpha^4)}{\beta(1-\alpha^2)} \quad (40)$$

(dropping the subscript i). When $\mathrm{v} \to 0$, this $\bar{\mu} = \mu(1 - c_s^2/c_d^2) = \mu/[2(1-\nu)]$ where, in the present undrained context, ν corresponds to ν_u. The combination $\gamma_i\beta_i - \alpha_i^4$ is the Rayleigh function for material i; that is, it vanishes (other than at $\mathrm{v} = 0$) at $\mathrm{v} = c_{Ri}$. Thus (40) shows that when the two half-spaces are identical, $\bar{\mu}(\mathrm{v}) = 0$ at their common Rayleigh speed c_R.

[37] When the half-spaces are dissimilar, a generalized Rayleigh speed c_{GR} is defined as the value of $\mathrm{v} > 0$, if such exists, for which $\bar{\mu}$ vanishes, i.e., $\bar{\mu}(c_{GR}) = 0$. Such a c_{GR} exists for modest dissimilarity of properties, typically for shear wave speeds different by less than 20–30%, a condition that often seems to be met for natural faults [*Andrews and Ben-Zion*, 1997]. When $\mathrm{v} = c_{GR}$, (33) shows that nonuniform slip does not alter the shear stress but (34) shows that it does alter the normal stress, in a tensile direction when $\mu^* > 0$. (Note that $\dot{\delta} = -\mathrm{v}d\delta/dx$, so that if $\dot{\delta} \geq 0$ and $\mathrm{v} > 0$, as implicitly assumed here, $d\delta/dx \leq 0$.) Exchanging the two half-spaces for one another or, equivalently, running the same slip history in the opposite direction along the interface, changes the sign of μ^*. In general, $\mu^* > 0$ if the wave speeds of material 1 are less than those of material 2, and vice versa; expressed differently [*Andrews and Ben-Zion*, 1997], normal stress clamping is decreased by nonuniform slip when the direction of propagation of the slip pattern is the same as the direction of the fault wall shear displacement in the slower material.

[38] *Weertman* [1980] suggested the possibility of, and *Adams* [1998] and *Rice* [1997] made explicit, simple solutions of (33) and (34), together with a Coulomb friction law $\sigma_{yx} = -f\sigma_{yy}$ with constant f, for which pulses of slip propagate at c_{GR}. They involve constant $\dot{\delta}$ in all sliding regions, when $0 < \sigma_{yx}^0 < -f\sigma_{yy}^0$ [see *Cochard and Rice*, 2000].

[39] The dissimilarity of elastic material away from the fault on the two sides, in addition to differences very near the fault predicted in the inset of Figure 1, alters the calculation of pore pressure described in Appendix B. In particular, the condition that the fault parallel strains are of equal magnitude, $\epsilon_{xx}^+ = -\epsilon_{xx}^-$, is no longer satisfied. Instead, a further analysis of the *Weertman* [1980] derivations leading to (33) and (34) shows that the extensional strains along the fault walls are

$$\epsilon_{xx}^+ = \epsilon_{xx,1} = \frac{1+\chi}{2}\frac{d\delta}{dx}\ , \quad \epsilon_{xx}^- = \epsilon_{xx,2} = -\frac{1-\chi}{2}\frac{d\delta}{dx} \quad (41)$$

where

$$\chi = (\Delta_1 - \Delta_2)/(\Delta_1 + \Delta_2) \quad (42)$$

χ reverses sign when we exchange one half-space for the other or, for a given position of the two materials, reverse the rupture propagation direction. In terms of those expressions, the result in the Appendix B for the pore pressure change on the fault plane, (B9) with (B10), is now altered to

$$p_f = -\frac{W(\mathrm{v})}{2}\frac{d\delta}{dx} \quad (43)$$

where

$$W(\mathrm{v}) = \frac{Z^+w^+ - Z^-w^-}{Z^+ + Z^-} + \chi(\mathrm{v})\frac{Z^+w^+ + Z^-w^-}{Z^+ + Z^-} - \mu^*(\mathrm{v})\frac{Z^+w^+/\mu^+ + Z^-w^-/\mu^-}{Z^+ + Z^-} \quad (44)$$

The first term in $W(\mathrm{v})$ is the same as before and independent of velocity. The second term, proportional to $\chi(\mathrm{v})$, results because the along fault extensional strains are no longer of identical magnitude on the two sides. The third term, proportional to $-\mu^\star(\mathrm{v})$, occurs because a nonzero change in σ_{yy} is induced in the bimaterial case. The coefficients of $\chi(\mathrm{v})$ and $-\mu^\star(\mathrm{v})$ are averages of w and w/μ, on the two sides of the fault, weighted by $Z^\pm$, respectively. Thus the equations for pore pressure and effective stress, corresponding to (33) and (34), are now

$$p(x) = p^0 - \frac{W(\mathrm{v})}{2}\frac{d\delta(x)}{dx}\ , \quad (45)$$

$$\sigma_{yy}(x) + p(x) = \left(\sigma_{yy}^0 + p^0\right) - \left(\mu^\star(\mathrm{v}) + \frac{W(\mathrm{v})}{2}\right)\frac{d\delta(x)}{dx}\ , \quad (46)$$

The latter shows that the proper measure of the propensity for slip to alter effective normal stress is the sum of the Weertman $\mu^\star$ and the poroelastic $W/2$ derived here. Either term may be positive or negative depending on the dissimilarity of properties adjacent to or farther from the slip zone, the direction of propagation and the sense of slip.

[40] As an example, consider material 1 (or plus) to be slightly more compliant and to have a slightly lower shear wave velocity than material 2 (or minus). In particular, $c_{s1} = 0.90c_{s2}$ and $c_{d1}/c_{s1} = c_{d2}/c_{s2} = \sqrt{3}$, corresponding to $\mu_1 = 0.75\mu_2$, $\rho_1 = 0.923\rho_2$ and $\nu_1 = \nu_2 = 0.25$. For this choice of Poisson's ratio (here to be interpreted as the undrained value), the Rayleigh wave speed in each material is 0.92 times the respective shear wave velocity. The generalized Rayleigh wave velocity, at which $\bar{\mu}(c_{GR}) = 0$, is $c_{GR} =$

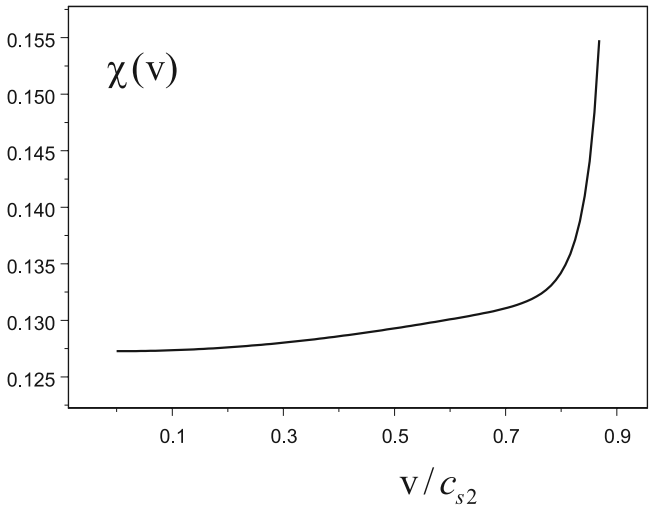

Figure 11. Plot of χ, equation (42), against v/c_{s2} up to $v = c_{GR}$ for $\mu_1 = 0.75\mu_2$, $\rho_1 = 0.923\rho_2$ and $\nu_1 = \nu_2 = 0.25$ so that $c_{s1} = 0.90c_{s2}$, $c_{d1}/c_{s1} = c_{d2}/c_{s2} = \sqrt{3}$ and $c_{GR} = 0.87c_{s2}$.

$0.87c_{s2}$ for these choices. Figure 11 plots χ (42), and Figure 12 plots $\mu^\star(v)/\mu_2$ as functions of velocity (divided by c_{s2}) up to c_{GR}. In this case both χ and $\mu^\star$ are positive, but exchanging the two materials or reversing the direction of slip introduces a negative sign. The magnitudes of both χ and μ increase as v approaches c_{GR}, but both are finite there ($\chi = 0.155$, $\mu^\star/\mu_2 = 0.178$).

[41] Figure 12 also plots values for $W/2\mu_2$ in order to compare the magnitudes of the bimaterial and porous media effects on alteration of the normal stress. As discussed in Appendix B, the properties entering W pertain to the near-fault material. Consequently, we choose the shear moduli, $\mu^+$and μ^-, entering W, (B10) with (B3), to be the same and equal to the average of the two shear moduli away from the fault, called μ here, and the Poisson's ratios again to be 0.25. Although B is often taken to be 0.9 for fault gouge [*Roeloffs and Rudnicki*, 1985; *Rudnicki*, 2001], we note in Appendix B that differences in properties on the two sides of the fault and the likelihood of greater damage near the fault tends to reduce the magnitude of the effective value of B although it may be of either sign. In addition, *Roeloffs* [1988] has discussed evidence for decreases in B with increasing effective stress, suggesting that smaller values are more appropriate for earthquake depths. Consequently, we have taken $B = 0.6$ for the material on both sides of the fault in plotting Figure 12. For this example, because the near properties are assumed to differ only in the values of the product $k\beta$, (44) simplifies to

$$W(v) = w\left\{\frac{Z^+ - Z^-}{Z^+ + Z^-} + \chi(v) - \mu^*(v)/\mu\right\} \qquad (47)$$

where $w^+ = w^- = w$ and $\mu^+ = \mu^- = \mu$. Results are shown in Figure 12 for values of the ratio $k^+\beta^+/k^-\beta^-$ equal to ∞, 10, 5, 2 and 1, 0.5, 0.2, 0.1 and 0. Since $\mu^\star(c_{GR})/\mu = 0.204$ exceeds $\chi(c_{GR}) = 0.155$, the sum of the latter two terms changes from positive to negative and causes the slight downturn in values of $W(v)/2$ as v approaches c_{GR}. Values of $k^+\beta^+/k^-\beta > 1$, so that the first (constant) term in W is >0, correspond to a more permeable compressive side of the fault; values less than one, making that first W term less than zero, correspond to a more permeable extensile side. (In general, that is, for different values of the shear modulus and Skempton's coefficients on the two sides of the fault, the sign of the first term in (44) for W depends on the full mismatch of properties, not just on the ratio $k^+\beta^+/k^-\beta^-$). Even if the materials bounding either side of the fault have identical properties, there is still a pore pressure induced if there is elastic mismatch farther from the fault (i.e., the contribution to the pore pressure then comes entirely from the latter two terms in (44)).

[42] Figure 12 shows that the alteration of the effective normal stress due to the induced pore pressure change may be of either sign and is comparable in magnitude to the alteration due to the elastic mismatch. The rapid increase of $\mu^\star/\mu_2$ as v approaches c_{GR} suggests, however, that the effect of the elastic mismatch will dominate near this limit, at least if B is not too large (larger values of B increase W) and mismatch in permeability is not extreme. If the half-spaces are exchanged so that the material in $y > 0$ is less compliant (has a greater shear wave speed), then the same plot (Figure 12) applies with the sign of the vertical axis reversed and the values of $k^+\beta^+/k^-\beta^-$ replaced by their reciprocals. Thus, in general, any of the terms due entering (44) may be positive or negative and the sign of the term due to near fault heterogeneity (first in (44)) may differ from that of terms due to elastic dissimilarity (sum of last two entering (44)). Therefore the sign and magnitude of the alteration of the effective normal stress depends not only on the elastic dissimilarity of the materials bounding the fault but also on their differences from the material very near the slip surface and the differences of the poroelastic properties of this

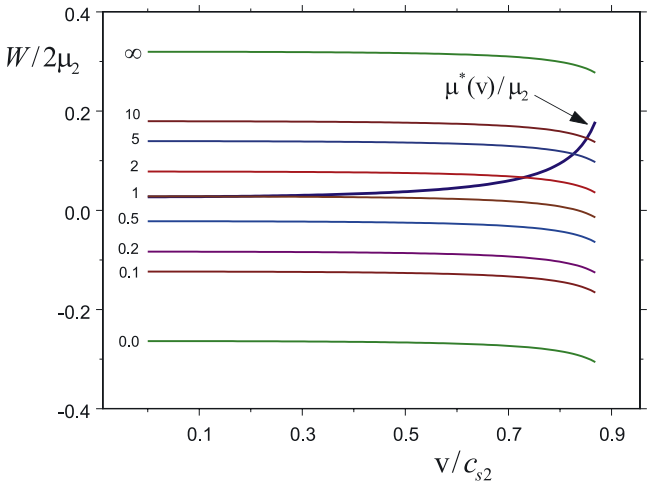

Figure 12. Plot of $\mu^*(v)/\mu_2$ against v/c_{s2} for the same elastic mismatch as in Figure 11: $\mu_1 = 0.75\mu_2$, $\rho_1 = 0.923\rho_2$ and $\nu_1 = \nu_2 = 0.25$ so that $c_{s1} = 0.90c_{s2}$, $c_{d1}/c_{s1} = c_{d2}/c_{s2} = \sqrt{3}$ and $c_{GR} = 0.87c_{s2}$. Remaining curves show $W/2\mu_2$ for different values of the ratio of the product of the near fault permeability and compressibility on the two sides of the fault, $k^+\beta^+/k^-\beta^-$. On both sides of the fault, the near fault shear modulus is taken to be the average of values farther from the fault, $B = 0.6$ and $\nu = 0.25$.

material on the two sides of the zone of concentrated sliding.

8. Discussion

[43] We have calculated the pore pressure induced by slip propagation for a model that idealizes recent detailed studies of fault zone structure [*Chester et al.*, 1993; *Chester and Chester*, 1998; *Lockner et al.*, 2000; *Wibberley and Shimamoto*, 2003; *Sulem et al.*, 2004; *Noda and Shimamoto*, 2005]. In particular, slip is modeled as occurring on a plane bounded by material with permeabilities and poroelastic properties that are different on each side of the slip plane and from the properties of the elastic material farther from the fault. The pore pressure change is the result of poroelastic deformation of the fault wall; changes due to inelastic porosity changes, dilation or compression, of the fault zone material would be in addition to these. Although the detailed calculations are carried out for the limiting case in which the compressive side of the slip zone is much more permeable than the extensile side, we have shown that they can be applied to the more elaborate model simply by modifying the effective value of the Skempton coefficient. In particular, by changing the sign of the effective Skempton's coefficient from positive to negative treats the case in which the extensile side of the fault is more permeable.

[44] Induced pore pressure by poroelastic compression discussed here is one of a number of mechanisms that have been suggested for dynamic weakening of slip resistance during earthquakes. These include thermal pressurization of pore fluid [*Lachenbruch*, 1980; *Mase and Smith*, 1987; *Garagash and Rudnicki*, 2003a, 2003b; *Garagash et al.*, 2005; *Rice*, 2006], flash heating of asperity contacts [*Rice*, 1999; *Tullis and Goldsby*, 2003; *Rice*, 2006] and others [*Sibson*, 1975; *Spray*, 1993, 1995; *Goldsby and Tullis*, 2002; *Chambon et al.*, 2002]. For the most part, these require rapid slip to generate heat sufficiently rapidly and relatively large slip to generate sufficiently high temperature (although *Segall and Rice* [2006] have shown that shear heating can be significant toward the end of the nucleation period, before slip velocities become seismic). Although the mechanism discussed here increases in magnitude with increasing velocity of propagation, it is also operative at small slip and at low velocities. Consequently, it may be a factor in allowing sufficient slip to occur long enough for other mechanisms to come into play or for preventing incipient slip from progressing, depending on the sign of the induced pore pressure change.

[45] The model provides a more general framework for considering the effects of material heterogeneities perpendicular to the fault on alterations of the effective normal stress. Previous studies [*Weertman*, 1980; *Andrews and Ben-Zion*, 1997; *Harris and Day*, 1997; *Cochard and Rice*, 2000; *Ben-Zion*, 2001; *Xia et al.*, 2005] have focused on the alteration of normal stress induced by inhomogeneous slip at the interface between elastic solids with different properties. The calculations here show that alterations of comparable magnitude in the effective normal stress can result from pore pressure changes induced by heterogeneous properties. More specifically, pore pressure changes result from differences in the permeability and poroelastic properties of the material on the two sides of the slip zone and from differences in the properties of this near fault material from that farther from the fault. Although parameter values are uncertain, a comparison of the magnitude of the two effects suggests that the effect due to nonuniform slip between different elastic solids may dominate as the rupture velocity approaches the generalized Rayleigh speed for the bimaterial, at least if the effective Skempton's coefficient is not too large, and the ratio of permeabilities is neither very large nor very small.

[46] Even when the effect due to elastic dissimilarity of material away from the fault is dominant, pore pressure changes due to near fault heterogeneity may augment or counteract the bimaterial effect. The sign of both effects can be positive or negative depending on the heterogeneity and the direction of slip and propagation. For example, the normal compressive stress is reduced by nonuniform slip when the direction of propagation of the slip distribution is the same as the direction of the fault wall displacement in the slower material. This reduction might, however, be diminished by a increase in effective compressive stress, due to a decrease in pore pressure, if the extensile side of the fault is more permeable. Thus the net effect of slip on the effective normal stress will depend on the details of the properties, both elastic and poroelastic, of the material bounding the zone of concentrated slip.

[47] Here the slip zone is assumed to occur at the interface of the two materials. Fault zone studies [*Chester et al.*, 1993; *Chester and Chester*, 1998; *Lockner et al.*, 2000; *Wibberley and Shimamoto*, 2003; *Sulem et al.*, 2004; *Noda and Shimamoto*, 2005] do show that the principal slip surface is very narrow, less than about 1 to 5 mm, and thus reasonably idealized as a planar discontinuity for some purposes. Such studies also show that the relatively impermeable fault core is a wider zone of 10 mm to hundreds of millimeters and bounded by a more permeable, damaged zone (grading to undamaged material farther from the fault). The model shown in the inset of Figure 1 is consistent with slip occurring at the boundary of these two zones. If only the effect of near fault heterogeneity is considered, and the slip zone is plausibly assumed to take a path of least resistance where the effective compressive normal stress is least, then the results here indicate that the slip zone will choose a path where the compressive side is more permeable. For the direction of slip (right lateral) and propagation (to the right) shown in Figure 1, this is consistent with the positive material being the less permeable ultracataclastic core and the negative material being the adjacent more permeable, damage layer. Of course, this simple picture could be complicated by a variety of other effects. Nevertheless, in a recent numerical study of the bimaterial effect, *Brietzke and Ben-Zion* [2006] found that when several slip surfaces were possible, the rupture tended to choose a material interface where the compressive normal stress was reduced. It is possible to speculate that when the pore pressure changes due to material heterogeneity are included, the rupture tends to choose the interface where the reduction of effective normal stress is greatest, though this is certainly an issue in need of further study.

[48] Another issue in need of further study is the effect of near fault damage induced by slip propagation. In contrast to the scenario of the previous paragraph, such damage may have an effect which, typically, acts oppositely to the

reduction of compressive normal stress due to far field elastic dissimilarity, by inducing negative pore pressure changes (suctions) along the slip surface. If there is no or only very small far field material dissimilarity, then the suctions will dominate and cause an increase in the effective normal compression, and hence partial stabilization of the fault. This possibility arises because a variety of studies [*Poliakov et al.*, 2002; *Kame et al.*, 2003; *Rice et al.*, 2005; *Andrews*, 2005; *Ben-Zion and Shi*, 2005] have shown that unless the direction of maximum principal stress is at an unusually shallow angle with the fault, say, less than ~25 degrees, then stresses predicted near the rupture front are expected to cause Mohr-Coulomb failure and damage preferentially on the extensile side of the slipping plane. Such preference is supported by field evidence [*Poliakov et al.*, 2002]. *Ben-Zion and Shi* [2005] have shown this same tendency for damage on the extensile side in simulations of rupture along an interface between elastically dissimilar materials. The spatial extent of the damaged zone is predicted to decrease with depth [*Rice et al.*, 2005] but the preferred side for damage remains. Presumably, this damage would increase the permeability on the extensile side whereas, conversely, compression of the other side may reduce the permeability there. The results here indicate that this effect, unless compensated by decrease of total compressive stress due to far field material dissimilarity, would decrease the pore pressure and hence increase the effective compressive stress and the energy required to propagate the fault. *Ben-Zion and Shi* [2005] have shown that including the effects of damage induced by rupture can modify and partially stabilize some aspects of the bimaterial effect. Further study of the effect on damage on altering the near fault permeability structure is needed.

9. Conclusion

[49] Interaction of pore fluid with material heterogeneity near the slip zone that is representative of that observed in fault zones can affect rupture propagation. An increase of pore pressure that reduces the effective compressive stress and facilitates slip propagation occurs if the compressive side of the slip zone (modeled as a plane) is more permeable than the tensile side; conversely, a decrease of pore pressure that increases the effective compressive stress and inhibits slip propagation occurs if tensile side is more permeable. Although a more complex and realistic model will undoubtedly alter the details of the calculations here, the main conclusion that near fault heterogeneity affects rupture propagation is unlikely to change. Understanding of how the particular effect studied here, pore pressure changes due to heterogeneous poroelastic properties, interacts with a variety of other effects must await further modeling and observational studies.

Appendix A: Details of the Solution

[50] The function $M(z)$ is analytic everywhere in the cut plane and approaches values on either side of the cut $-L \leq x \leq 0$ that are related by (15). The solution proceeds by first finding a function that satisfies the homogeneous equation ((15) with zero right hand side). Although there is a formal procedure for this [*Muskhelishvili*, 1992; *England*, 2003], it is straightforward to verify that the complex function $z/(z+L)^{(1/2)-\varepsilon}$, with branch cut taken on $y = 0$, $-L \leq x \leq 0$, satisfies (15) with zero right side.

[51] Because any analytic function multiplied by this function is also a solution to the homogeneous equation and because it will be convenient to have a solution that decays as z^{-1} as $|z| \rightarrow \infty$, we take the homogeneous solution to be

$$\chi(z) = \frac{1}{(z+L)^{\frac{1}{2}-\varepsilon}(z)^{\frac{1}{2}+\varepsilon}} \tag{A1}$$

Dividing both sides of (15) by $\chi^+(x)$ and using the homogeneous equation yields

$$\left[\frac{M(x)}{\chi(x)}\right]^+ - \left[\frac{M(x)}{\chi(x)}\right]^- = \frac{2g(x)}{(1+ki)\chi^+(x)} \tag{A2}$$

Equation (A2) has the solution [*Muskhelishvili*, 1992; *England*, 2003]

$$\frac{M(z)}{\chi(z)} = \frac{1}{\pi i(1+ki)} \int_{-L}^{0} \frac{g(t)}{\chi^+(t)} \frac{dt}{t-z} + \frac{A}{\pi} \tag{A3}$$

where A is a constant.

[52] The constant A is determined by the condition that the singularity in $M(z)$ vanish as $z \rightarrow 0$. This results from the physical requirement that the slip weakening zone causes the relative displacement to vanish smoothly at the edge of the slipping zone. Setting $z^{(1/2)+\varepsilon}M(z)$ equal to zero in the limit $z \rightarrow 0$ yields

$$A = \cos(\pi\varepsilon) \int_{-L}^{0} \frac{g(t)(L+t)^{\frac{1}{2}-\varepsilon}}{(-t)^{\frac{1}{2}-\varepsilon}} dt \tag{A4}$$

where $\cos(\pi\varepsilon) = 1/\sqrt{1+k^2}$. The slip must, however, also cease smoothly at the trailing edge of the slipping zone, $x = -L$. This leads to the additional requirement on A that results from setting $(z+L)^{(1/2)-\varepsilon}M(z)$ equal to zero in the limit $z \rightarrow -L$:

$$A = -\cos(\pi\varepsilon) \int_{-L}^{0} \frac{g(t)(-t)^{\frac{1}{2}+\varepsilon}}{(t+L)^{\frac{1}{2}+\varepsilon}} dt \tag{A5}$$

Equating the two expressions (A4) and (A5) for A yields the following constraint on $g(t)$

$$\int_{-L}^{0} \frac{g(t)}{(-t)^{\frac{1}{2}-\varepsilon}(t+L)^{\frac{1}{2}+\varepsilon}} dt = 0 \tag{A6}$$

Substituting from (A4) for A and $\chi(z)$ into (A3) and then using the constraint equation (A6) yield

$$M(z) = -\frac{\cos(\pi\varepsilon)}{\pi} z^{\frac{1}{2}-\varepsilon}(z+L)^{\frac{1}{2}+\varepsilon} \int_{-L}^{0} \frac{g(t)dt}{(-t)^{\frac{1}{2}-\varepsilon}(t+L)^{\frac{1}{2}+\varepsilon}(t-z)} \tag{A7}$$

When $g(t)$ is substituted from (8), the integral in the term multiplying $(\sigma^0_{xy} - \tau_r)$ can be done using contour integration by means similar to those described by RSP. The resulting expression for $M(z)$ is (16) in the text. The $\mathrm{Im}\{M^+(x)\}$, which is needed to obtain the pore pressure can be calculated numerically directly from (16) and is also given by

$$\mathrm{Im}\{M^+(x)\} = \left(\tau_p - \tau_r\right)\frac{(\cos(\pi\varepsilon))^2}{\pi R}(-x)^{\frac{1}{2}-\varepsilon}(L+x)^{\frac{1}{2}+\varepsilon} \cdot \int_0^1 \frac{(1-s)ds}{s^{\frac{1}{2}-\varepsilon}[(L/R)-s]^{\frac{1}{2}+\varepsilon}[s+(x/R)]} \tag{A8}$$

where the change of variable $t = -sR$ has been used in the integral.

A1. Stress Drop

[53] Substitution of the expression for g into (A6) gives a relation between the ratio of the driving stress $(\sigma^0_{xy} - \tau_r)$ to the cohesive zone stress drop $(\tau_p - \tau_r)$ and the scaled cohesive zone size R/L:

$$\frac{\sigma^0_{xy} - \tau_r}{\tau_p - \tau_r} = \frac{\int_{-R}^0 \left[(1+t/R)/(-t)^{\frac{1}{2}-\varepsilon}(t+L)^{\frac{1}{2}+\varepsilon}\right]dt}{\int_{-L}^0 \left[1/(-t)^{\frac{1}{2}-\varepsilon}(t+L)^{\frac{1}{2}+\varepsilon}\right]dt} \tag{A9}$$

The integral in the denominator can be evaluated by converting it to a contour integral around the branch cut $-L \le x < 0$ in the complex plane and the result is

$$\int_{-L}^0 \left[1/(-t)^{\frac{1}{2}-\varepsilon}(t+L)^{\frac{1}{2}+\varepsilon}\right]dt = \pi/\cos(\pi\varepsilon) \tag{A10}$$

Using (A10) and the substitution $p = -t/R$ in the integral in the numerator of (A9) gives (22) of the text.

A2. Relative Slip Displacements

[54] The variation of the relative displacement can be written as

$$\frac{\partial\delta}{\partial x}(x) = 2\epsilon_{xx}(x,0^+) = \frac{(1-\nu_u)}{\mu}\Delta\sigma_{xx}(x,0^+) \tag{A11}$$

Substituting for $\Delta\sigma_{xx}(x, 0^+)$ from (9a) and using the identity (with Poisson's ratio taken as the undrained value)

$$1 - \nu_u = \frac{\left(1-\alpha_s^2\right)}{2\left(\alpha_d^2 - \alpha_s^2\right)} \tag{A12}$$

give

$$\frac{\partial\delta}{\partial x}(x) = \frac{2}{\mu F(\mathrm{v})}\mathrm{Im}\{M^+(x)\} \tag{A13}$$

where $F(\mathrm{v})$ is defined following (24). Integrating and noting that $\delta = 0$ at $x = 0$ give

$$\delta(x) = \frac{2\left(\tau_p - \tau_r\right)}{\pi\mu F(\mathrm{v})}\cos(\pi\varepsilon)\int_0^x H\left(\frac{s}{R};\frac{R}{L}\right)ds \tag{A14}$$

where

$$\mathrm{Im}\{M^+(x)\} = \frac{1}{\pi}\left(\tau_p - \tau_r\right)\cos(\pi\varepsilon)H\left(\frac{x}{R};\frac{R}{L}\right) \tag{A15}$$

[55] Evaluating $\delta(x)$ from (A14) at $x = -L$ gives the total, locked-in displacement that has accumulated at the trailing edge of the slip zone δ_T. This total displacement can, however, be obtained directly by the same arguments used by RSP and *Poliakov et al.* [2002]. They show that δ_T is proportional to A and is given by

$$\delta_T = \frac{2A\alpha_s\left(1-\alpha_s^2\right)}{\mu D} \tag{A16}$$

Using (A4) for A and substituting the expression for $g(t)$ from (8) yield

$$A = \left(\tau_p - \tau_r\right)\cos(\pi\varepsilon)\int_{-R}^0 \frac{(1+t/R)(L+t)^{\frac{1}{2}-\varepsilon}}{(-t)^{\frac{1}{2}-\varepsilon}}dt - \left(\sigma^0_{xy} - \tau_r\right)\cos(\pi\varepsilon)\int_{-L}^0 \frac{(L+t)^{\frac{1}{2}-\varepsilon}}{(-t)^{\frac{1}{2}-\varepsilon}}dt \tag{A17}$$

If the second integral is denoted I, then dI/dL is equal to $(1/2 - \varepsilon)$ times the integral in (A10). Using this result and (22) and combining the integrals make it possible to write A as

$$A = L\left(\frac{R}{L}\right)^{\frac{1}{2}+\varepsilon}\Delta\left(\frac{R}{L};\varepsilon\right) \tag{A18}$$

where $\Delta(R/L;\ \varepsilon)$ is given by (25). Substituting (A18) into (A16) gives (24) of the text. This expression for δ_T agrees with (A14) evaluated at $x = -L$.

Appendix B: Pore Pressure at the Fault Plane

[56] In the main text the fault has sometimes been described, for simplicity, as a completely impermeable plane of displacement discontinuity in a uniform material, with pore pressure on the compressed side entering the friction law. Although it is a reasonable approximation to assume uniform material properties at some distance away from the fault, detailed examinations of fault zones [*Chester et al.*, 1993; *Chester and Chester*, 1998; *Wibberley and Shimamoto*, 2003] show that the fault walls are often bordered by materials that are different from each other and from the uniform material farther away. In this Appendix, we show the effect of these different near fault properties, including the actual finite, if small, permeabilities of the materials involved (leading to a continuous pore pressure variation across the fault plane), can be included by modifying a parameter of the analysis based on discontinuous pressure at an impermeable plane in a uniform material. In particular, we assume that these regions of different properties bordering the fault are thin enough that they can be considered to undergo a uniform x direction strain $\varepsilon^+_{xx}(t)$ on one side of the fault and an equal and opposite strain $\varepsilon^-_{xx}(t) = -\varepsilon^+_{xx}(t)$ on the other side (Figure 1, inset). Because those bordering zones are presumed to be thin (compared, say, to the along-strike

length scales R and L), the strains will be essentially identical to those calculated along the fault walls for the uniform material model in the body of the paper. These fault-parallel strains are related to the slip rate $\dot{\delta}$ at a fixed position x and rupture velocity v by

$$\varepsilon_{xx}^{+}(t) = -\varepsilon_{xx}^{-}(t) = -\dot{\delta}/2\mathrm{v} \tag{B1}$$

where the compressive side of the fault is assumed to be $y > 0$. (Because the solution is steady state $2\varepsilon_{xx}^{+} = \partial\delta/\partial x = -(1/\mathrm{v})\partial\delta/\partial t$ and this expression is consistent with (A11).) The strains are calculated as in the main text, based on the solution for an impermeable fault plane in uniform material.

[57] The hydraulic diffusivity α_{hy} of fault gouge at representative seismogenic depths is generally estimated as being in the range of $1-10$ mm^2/s [*Rice*, 2006], and the duration t of slip at a point in large earthquakes is typically of the order of 1 s for every 1 m of slip [*Heaton*, 1990]. Thus the thickness of the region over which fluid diffusion smooths out the discontinuity of the impermeable fault model, of the order of a few times $\sqrt{\alpha_{hy}t}$, will not generally be larger than a few tens of millimeters. Thus we are concerned here with the properties and poromechanical response of border regions of that order of thickness along the fault walls.

[58] Now consider a magnified view of such border regions along the fault plane, so that they appear as two half planes subjected to a uniform x direction strain $\varepsilon_{xx}^{+}(t)$ in $y > 0$ and an equal and opposite strain $\varepsilon_{xx}^{-}(t) = -\varepsilon_{xx}^{+}(t)$ in $y < 0$. The two half-spaces are assumed to be deforming under plane strain conditions ($\varepsilon_{zz} = 0$) and are subjected to the same fault normal stress σ_{yy}, which remains constant during slip. The shear stress σ_{xy} does vary but that does not affect the pore pressure under these conditions, assuming that the border regions are isotropic, or are aleotropic with principal directions aligned with the x and y directions. What is the pore pressure $p_f(t)$ induced at the fault plane $y = 0$?

[59] To answer this question, first imagine that the plane $y = 0$ is completely impermeable. Then the pore pressure changes $p_0^{\pm}(t)$ from the ambient value are uniform in each half-space and given by

$$p_0^{\pm}(t) = -w^{\pm}\varepsilon_{xx}^{\pm}(t) \tag{B2}$$

The $w^{\pm}$ for each poroelastic half-space for undrained, plane strain conditions and constant σ_{yy} is [*Rice and Cleary*, 1976]

$$w^{\pm} = 2\mu^{\pm}\frac{B^{\pm}\left(1+\nu_u^{\pm}\right)}{3\left(1-\nu_u^{\pm}\right)} \tag{B3}$$

when the border regions are isotropic, where $\pm$ refer to the local, near fault properties in $y \gtrless 0$. The factor $B^{\pm}(1+\nu_u^{\pm})/3(1-\nu_u^{\pm})$ attains its maximum value, unity, for $B^{\pm} = 1$ and $\nu_u^{\pm} = 1/2$ which is the case when both solid and fluid constituents are incompressible. Note that the near fault strains $\varepsilon_{xx}^{\pm}(t)$ (assumed spatially uniform in this magnified view) are related to $\sigma_{xx}^{\pm}$ from the analysis of the text by the uniform properties μ and ν_u away from the fault, i.e.,

$$\varepsilon_{xx}^{\pm}(t) = (1-\nu_u)\sigma_{xx}^{\pm}/2\mu \tag{B4}$$

[60] If the plane $y = 0$ is not completely impermeable, then spatially dependent pore pressure changes $p(y, t)$ will develop in each half-space. The difference between these fields and the uniform, undrained pore pressure (B2) satisfies a homogeneous diffusion equation in each half-space [e.g., *Rice and Cleary*, 1976]:

$$\frac{\partial}{\partial t}\left[p(y,t) - p_0^{\pm}(t)\right] = \alpha_{\mathrm{hy}}^{\pm}\frac{\partial^2}{\partial y^2}\left[p(y,t) - p_0^{\pm}(t)\right] \tag{B5}$$

where $\pm$ again refer to $y > 0$ and $y < 0$, and $\alpha_{\mathrm{hy}}^{\pm}$ are the hydraulic diffusivities. The hydraulic diffusivities can be written as $k^{\pm}/\eta_f\beta^{\pm}$, where $k^{\pm}$ are the permeabilities, $\beta^{\pm}$ are the storage coefficients and η_f is the fluid viscosity, which is the same in both half-spaces. The diffusion equations must be solved in the two domains $y > 0$ and $y < 0$, subject to two conditions at the interface $y = 0$. The first is that the pore fluid pressures be the same (i.e., p is continuous),

$$p(y = 0^{+}, t) = p(y = 0^{-}, t) = p_f(t) \tag{B6}$$

where $p_f(t)$ is the pore pressure on the fault that we seek. The second is the fluid flux across the interface (given by Darcy's law) is continuous

$$k^{+}\frac{\partial p}{\partial y}(y = 0^{+}, t) = k^{-}\frac{\partial p}{\partial y}(y = 0^{-}, t) \tag{B7}$$

[61] Solution by Laplace transform shows that the pore pressure on the fault is given by

$$p_f(t) = \frac{Z^{+}p_0^{+}(t) + Z^{-}p_0^{-}(t)}{Z^{+} + Z^{-}} \tag{B8}$$

where $Z^{\pm} = \sqrt{k^{\pm}\beta^{\pm}}$. Substituting from (B2) and using $\varepsilon_{xx}^{-}(t) = -\varepsilon_{xx}^{+}(t)$ gives

$$p_f(t) = -W\varepsilon_{xx}^{+}(t) = -\frac{W}{2}\frac{d\delta}{dx} \tag{B9}$$

where

$$W = \frac{Z^{+}w^{+} - Z^{-}w^{-}}{Z^{+} + Z^{-}} \tag{B10}$$

In the body of the paper we generalize the last pair of equations to the case of two elastically dissimilar half-spaces adjoining the fault, each lined with a narrow fault-bordering layer whose poroelastic properties define the $w^{\pm}$ and $Z^{\pm}$ as here. Substituting (B4) yields

$$p_f(t) = -\frac{1}{3}(BW/w)(1+\nu_u)\Delta\sigma_{xx}^{+}(t) \tag{B11}$$

where w here is defined as in (B3), B is the Skempton coefficient, and both are based on the properties farther from the fault. Thus the fault pore pressure is defined by the same relation as in a homogeneous material

$$p_f(t) = -\frac{1}{3}B'(1+\nu_u)\Delta\sigma_{xx}^{+}(t) \tag{B12}$$

where $B' = BW/w$. Note, however, from (B10) that W need not be positive, and thus B' may be of either sign, depending on material properties in the two border regions. With this interpretation of B as B', the solution for a uniform material with an impermeable fault plane, given in the main text, applies as well for the more realistic model of this Appendix. The case $B' > 0$ corresponds to weakening the fault by induced pore pressure, and $B' < 0$ to strengthening by induced pore suction.

[62] As a simple case, assume that all the near fault properties, except for the permeabilities, are identical to those of the homogeneous material farther from the fault. Then B' reduces to

$$B' = B\left\{\frac{1-\sqrt{k^-/k^+}}{1+\sqrt{k^-/k^+}}\right\} \tag{B13}$$

Hence, when the permeability of the extensional side is much less than that of the compressional, $k^- \ll k^+$, then $B' = B$. If $k^-/k^+ = 10^{-2}$, which might be representative of having ultracataclasite on the extensional side and a coarser gouge or densely cracked material from the damaged fault core on the compressional side, based on properties inferred from *Lockner et al.* [2000] and *Wibberley and Shimamoto* [2003], then $B' \simeq 0.82B$; if $k^-/k^+ = 10^{-1}$, $B' \simeq 0.52B$. So the effect of decreasing permeability of the part of the fault core on the extensional side is to reduce the effective value of Skempton's coefficient in the solution. If the extensional side is the more permeable, which is the case generally expected based on where Mohr-Coulomb plasticity and damage is expected to occur most extensively near the rupture front, then $k^- > k^+$, and then $B' < 0$ and suction rather than pressure is induced on the fault plane.

[63] More generally, if all properties of the border regions differ from those farther away, so that (B13) does not apply, but if it is nevertheless the case that the extensional side is essentially impermeable compared to the compressive, $k^-/k^+ \to 0$, then

$$B' = B^+\frac{\mu^+}{\mu}\left[\frac{\left(1+\nu_u^+\right)/\left(1-\nu_u^+\right)}{(1+\nu_u)/(1-\nu_u)}\right] \tag{B14}$$

The same expression for B' results, except that it is preceded by a minus sign and all plus superscripts are changed to minus, in the case for which the compressive side is essentially impermeable compared to the extensional, $k^-/k^+ \to \infty$. The term in brackets involving Poisson's ratio varies by at most a factor of three. For $\nu_u^+ = 0.4$ and $\nu_u = 0.2$, this bracket is 1.55. Thus, in these cases with one side being essentially impermeable compared to the other, B' is roughly equal to the near fault Skempton's coefficient B^+ reduced by the ratio of the shear modulus near the fault to that farther away, or to $-B^-$ reduced by a similar factor. The effect is to reduce the magnitude of the effective value of B, although the reduction might be partly offset by an increase in the undrained Poisson's ratio in the near fault material.

[64] **Acknowledgments.** This work was begun during September 2003 at the Isaac Newton Institute for Mathematical Sciences, University of Cambridge, England, while both authors were participants in the Program on Granular and Particle Laden Flows. We are grateful for the support of the institute and the organizers. We thank Eric Dunham providing a check of some of the numerical calculations and also for helping uncover an error in our original analysis of the effects of elastic dissimilarity. J.W.R. is grateful for support from the Kavli Institute for Theoretical Physics, Santa Barbara, while participating in the program on Granular Physics and from the U.S. Department of Energy, Office of Basic Energy Science, Geosciences Research Program. J.R.R. is grateful for support of NSF grants EAR-0125709 and 0510193 and of the NSF/USGS Southern California Earthquake Center, funded by NSF Cooperative Agreement EAR-0106924 and USGS Cooperative Agreement 02HQAG0008 (this is SCEC contribution 932).

References

Adams, G. G. (1995), Self-excited oscillations of two elastic half-spaces sliding with a constant coefficient of friction, *J. Appl. Mech.*, *62*, 867–872.

Adams, G. G. (1998), Steady sliding of two elastic half-spaces with friction reduction due to interface stick-slip, *J. Appl. Mech.*, *65*, 470–475.

Andrews, D. J. (2005), Rupture dynamics with energy loss outside the slip zone, *J. Geophys. Res.*, *110*, B01307, doi:10.1029/2004JB003191.

Andrews, D. J., and Y. Ben-Zion (1997), Wrinkle-like slip pulse on a fault between different materials, *J. Geophys. Res.*, *102*, 553–571.

Ben-Zion, Y. (2001), Dynamic ruptures in recent models of earthquake faults, *J. Mech. Phys. Solids*, *49*, 2209–2244.

Ben-Zion, Y., and Z. Shi (2005), Dynamic rupture on a material interface with spontaneous generation of plastic strain in the bulk, *Earth Planet. Sci. Lett.*, *236*, 486–496.

Brietzke, G., and Y. Ben-Zion (2006), Examining tendencies of in-plane rupture to migrate to material interfaces, *Geophys. Int. J.*, *167*, doi:10.1111/j.1365-246X.2006.03137.x.

Brener, E., S. Malinin, and V. Marchenko (2005), Fracture and friction: Stick-slip motion, *Eur. Phys. J. E*, *17*, 101–113, doi:10.1140/epje/i2004-10112-3.

Chambon, G., J. Schmittbuhl, and A. Corfdir (2002), Laboratory gouge friction: Seismic-like slip weakening and secondary rate- and state-effects, *Geophys. Res. Lett.*, *29*(10), 1366, doi:10.1029/2001GL014467.

Chester, F. M., and J. S. Chester (1998), Ultracataclasite structure and friction processes of the Punchbowl Fault, San Andreas System, California, *Tectonophysics*, *295*(1–2), 199–221.

Chester, F. M., J. P. Evans, and R. L. Biegel (1993), Internal structure and weakening mechanisms of the San Andreas fault, *J. Geophys. Res.*, *98*, 771–786.

Cochard, A., and J. R. Rice (2000), Fault rupture between dissimilar materials: Ill-posedness, regularization and slip-pulse response, *J. Geophys. Res.*, *105*, 25,891–25,907.

Comninou, M. (1978), The interface crack in a shear field, *J. Appl. Mech.*, *45*(2), 287–290.

Dunham, E. M., and R. J. Archuleta (2005), Near-source ground motion from steady state dynamic rupture pulses, *Geophys. Res. Lett.*, *32*, L03302, doi:10.1029/2004GL021793.

England, A. H. (2003), *Complex Variable Methods in Elasticity*, Dover, Mineola, N. Y.

Garagash, D. I., and J. W. Rudnicki (2003a), Shear heating of a fluid-saturated slip-weakening dilatant fault zone: 1. Limiting regimes, *J. Geophys. Res.*, *108*(B2), 2121, doi:10.1029/2001JB001653.

Garagash, D. I., and J. W. Rudnicki (2003b), Shear heating of a fluid-saturated slip-weakening dilatant fault zone: 2. Quasi-drained regime, *J. Geophys. Res.*, *108*(B10), 2472, doi:10.1029/2002JB002218.

Garagash, D. I., D. G. Schaeffer, and J. W. Rudnicki (2005), Effect of rate dependence in shear heating of a fluid-saturated fault zone, in *Poromechanics III-Biot Centennial (1905–2005), Proceedings, 3rd Biot Conference on Poromechanics*, edited by Y. Abousleiman, A. H.-D. Cheng, and F.-J. Ulm, pp. 789–794, A. A. Balkema, Brookfield, Vt.

Goldsby, D. L., and T. E. Tullis (2002), Low frictional strength of quartz rocks at subseismic slip rates, *Geophys. Res. Lett.*, *29*(17), 1844, doi:10.1029/2002GL015240.

Harris, R., and S. M. Day (1997), Effects of a low velocity zone on a dynamic rupture, *Bull. Seismol. Soc. Am.*, *87*, 1267–1280.

Heaton, T. H. (1990), Evidence for and implications of self-healing pulses of slip in earthquake rupture, *Phys. Earth Planet. Inter.*, *64*, 1–20.

Kame, N., J. R. Rice, and R. Dmowska (2003), Effects of prestress state and rupture velocity on dynamic fault branching, *J. Geophys. Res.*, *108*(B5), 2265, doi:10.1029/2002JB002189.

Lachenbruch, A. H. (1980), Frictional heating, fluid pressure, and the resistance to fault motion, *J. Geophys. Res.*, *85*, 6097–6112.

Lockner, D., H. Naka, H. Tanaka, H. Ito, and R. Ikeda (2000), Permeability and strength of core samples from the Nojima fault of the 1995 Kobe earthquake, in *Proceedings of the International Workshop on the Nojima Fault Core and Borehole Data Analysis, Tsukuba, Japan, Nov 22–23, 1999*, edited by H. Ito et al., *U.S. Geol. Surv. Open File Rep., 00-129*, 147–152.

Mase, C. W., and L. Smith (1987), Effects of frictional heating on the thermal, hydrologic, and mechanical response of a fault, *J. Geophys. Res.*, *92*, 6249–6272.

Muskhelishvili, N. I. (1992), *Singular Integral Equations*, 2nd ed., Dover, Mineola, N. Y.

Noda, H., and T. Shimamoto (2005), Thermal pressurization and slip-weakening distance of a fault: An example of the Hanaore fault, southwest Japan, *Bull. Seismol. Soc. Am.*, *95*(4), 1224–1233.

Palmer, A. C., and J. R. Rice (1973), The growth of slip surfaces in the progressive failure of over-consolidated clay, *Proc. R. Soc. London, Ser. A*, *332*, 527–548.

Poliakov, A. N. B., R. Dmowska, and J. R. Rice (2002), Dynamic shear rupture interactions with fault bends and off-axis secondary faulting, *J. Geophys. Res.*, *107*(B11), 2295, doi:10.1029/2001JB000572.

Rice, J. R. (1997), Slip pulse at low driving stress along a frictional fault between dissimilar media (abstract), *Eos Trans. AGU*, *78*(46), Fall Meet. Suppl., F464.

Rice, J. R. (1999), Flash heating at asperity contacts and rate-dependent friction (abstract), *Eos Trans. AGU*, *80*(46), Fall Meeting Suppl., F681.

Rice, J. R. (2006), Heating and weakening of faults during earthquake slip, *J. Geophys. Res.*, *111*, B05311, doi:10.1029/2005JB004006.

Rice, J. R., and M. P. Cleary (1976), Some basic stress diffusion solutions for fluid-saturated elastic porous media with compressible constituents, *Rev. Geophys.*, *14*, 227–241.

Rice, J. R., C. G. Sammis, and R. Parsons (2005), Off-fault secondary failure induced by a dynamic slip-pulse, *Bull. Seismol. Soc. Am.*, *95*(1), 109–134, doi:10.1785/0120030166.

Roeloffs, E. A. (1988), Fault stability changes induced beneath a reservoir with cyclic variations in water level, *J. Geophys. Res.*, *93*, 2107–2124.

Roeloffs, E. A., and J. W. Rudnicki (1985), Coupled deformation diffusion effects on water-level changes due to propagating creep events, *Pure Appl. Geophys.*, *122*, 560–582.

Rudnicki, J. W. (2001), Coupled deformation-diffusion effects in the mechanics of faulting and failure of geomaterials, *Appl. Mech. Rev.*, *54*(6), 483–502.

Rudnicki, J. W., and D. A. Koutsibelas (1991), Steady propagation of plane strain shear cracks on an impermeable plane in an elastic diffusive solid, *Int. J. Solids Struct.*, *27*, 205–225.

Segall, P., and J. R. Rice (2006), Does shear heating of pore fluid contribute to earthquake nucleation?, *J. Geophys. Res.*, *111*, B09316, doi:10.1029/2005JB004129.

Sibson, R. H. (1975), Generation of pseudotachylyte by ancient seismic faulting, *Geophys. J. R. Astron. Soc.*, *43*, 775–794.

Spray, J. G. (1993), Viscosity determinations of some frictionally generated silicate melts: Implications for fault zone rheology at high strain rates, *J. Geophys. Res.*, *98*, 8053–8068.

Spray, J. G. (1995), Pseudotachylyte controversy: Fact or friction?, *Geology*, *23*, 1119–1122.

Sulem, J., I. Vardoulakis, H. Ouffroukh, M. Boulon, and J. Hans (2004), Experimental characterization of the thermo-poro-mechanical properties of the Aegion Fault gouge, *C. R. Geosci.*, *336*(4–5), 455–466.

Tullis, T. E., and D. Goldsby (2003), Flash melting of crustal rocks at almost seismic slip rates (abstract), *Eos Trans. AGU*, *84*(46), Fall Meeting Suppl., Abstract S51B-05.

Weertman, J. (1980), Unstable slippage across a fault that separates elastic media of different elastic constants, *J. Geophys. Res.*, *85*, 1455–1461.

Wibberley, C. A. J., and T. Shimamoto (2003), Internal structure and permeability of major strike-slip fault zones: The Median Tectonic Line in Mie Prefecture, southwest Japan, *J. Struct. Geol.*, *25*, 59–78.

Xia, K., A. J. Rosakis, H. Kanamori, and J. R. Rice (2005), Laboratory earthquakes along inhomogeneous faults: Directionality and supershear, *Science*, *308*(5722), 681–684.

J. R. Rice, Department of Earth and Planetary Sciences, Harvard University, 224 Pierce Hall, 29 Oxford Street, Cambridge, MA 02138, USA. (rice@esag.deas.harvard.edu)

J. W. Rudnicki, Department of Civil and Environmental Engineering, Northwestern University, Evanston, IL 60208-3109, USA. (jwrudn@northwestern.edu)